The response of Li and Mg isotopes to rain events in a highly-weathered catchment

David M. Fries[1], Rachael H. James[1], Céline Dessert[2], Julien Bouchez[2], Aurélien Beaumais[1, 3], Christopher R. Pearce[4]

[1]School of Ocean and Earth Science, National Oceanography Centre Southampton, University of Southampton Waterfront Campus, European Way, Southampton SO14 3ZH, UK

[2]Institut de Physique du Globe de Paris (IPGP), Sorbonne Paris Cité, Université Paris Diderot, CNRS, Paris, France

[3]DEN – Service d'Etudes Analytiques et de Réactivité des Surfaces (SEARS), CEA, Université Paris-Saclay, F-91191 Gif sur Yvette, France

[4]Marine Geoscience, National Oceanography Centre, Southampton SO14 3ZH, UK

ABSTRACT

Storms are responsible for up to ~50 % of total annual rainfall on tropical islands and result in rapid increases in discharge from rivers. Storm events are, however, notoriously under-sampled and their effects on weathering rates and processes are poorly constrained. To address this, we have undertaken high-frequency sampling of Quiock Creek catchment, a Critical Zone Observatory located in Guadeloupe, over a period of 21 days, encompassing several storm events. Chemical and isotopic (Li and Mg) analyses of different critical zone reservoirs (throughfall, soil pore water, groundwater and river water) were used to assess the interactions between rock, water and secondary minerals. The Li concentrations and δ^7Li values of these different reservoirs range from 14 to 95 nmol/kg and 1.8 to 16.8‰, respectively. After several rain events, the average δ^7Li value (13.3‰) of soil solutions from the lower part of the soil profile (> ~150 cm below the surface) was unchanged, whereas in the upper part of the profile δ^7Li values increased by ~2 - 4‰ due to increased contribution from throughfall. By contrast, the δ^{26}Mg value of soil waters in the upper part of the soil profile were not significantly affected by the rain events with an average value of -0.90‰. The δ^{26}Mg values of the different fluid reservoirs were generally close to the value of throughfall (~ -0.90‰), but higher δ^{26}Mg values (up to -0.58‰) were measured in the deeper parts

of the soil profile, whereas groundwaters that have a long residence time had lower δ^{26}Mg values (down to -1.48‰). These higher and lower values are attributed to, respectively, adsorption/desorption of light Mg isotopes on/from the surface of clay minerals. The δ^{7}Li value of the river waters was ~9.3‰, with a Li concentration of 60 µmol/kg, but during a storm these values decreased to, respectively, 7.8‰ and 40 µmol/kg. This change in δ^{7}Li is consistent with an increased contribution of Li from the soil solution. Thus, even in highly weathered catchments, changes in hydrological conditions can have a significant impact on weathering processes and therefore the composition of river waters delivered to the ocean.

KEYWORDS

Lithium isotopes; Magnesium isotopes; Tropical rivers; Weathering ; Critical Zone; Hydrology

HIGHLIGHTS

- **Series of rain events reduces the δ^{7}Li value of river waters in a tropical catchment**
- **Mg isotope composition of soil solutions is controlled by adsorption and desorption processes.**
- **Storm events have little effect on δ^{26}Mg values because most of the Mg in the studied catchment is supplied by throughfall.**

1. Introduction

Weathering processes drive soil and landscape formation, soil nutrient cycling and control the delivery of chemical elements from the continents to the oceans (Gaillardet et al., 1999; Millot et al., 2002). The chemical composition of water compartments in the critical zone is also strongly influenced by hydrology (Maher, 2011); in some rivers element concentrations do not vary with discharge, so elemental fluxes are determined primarily by the water flux, whereas in other rivers, element concentrations decrease with increasing discharge indicating that dilution is the principal control and elemental fluxes remain constant (Godsey et al., 2009). Concentration-discharge relationships are controlled by various parameters, including: water saturation in the soil (Godsey et al., 2009); the interplay between fluid residence time, the thermodynamics and kinetics of water-rock interactions (Maher, 2011); exchange reactions (Clow and Mast, 2010); and mixing between different subsurface or surface water bodies (Calmels et al., 2011) (Bouchez et al., 2017). During extreme hydrological events such as storms, chemical weathering fluxes are likely to be highly dependent on changes in water residence time (Benettin et al., 2017), as well as on the mobilization of “old pockets” of subsurface/deep water that has a distinct chemical composition linked to its long residence time. However, even in small, relatively homogeneous catchments, sampling of rivers (e.g. weekly or monthly) provides only a snapshot of the water-rock interactions. Storm events are often undersampled although they can contribute up to 50% of the total annual water export over very short periods of time (Larsen and Simon, 1993). In areas where the hydrological cycle is highly variable, high-frequency sampling is thus needed to fully evaluate weathering fluxes and gain better insight into weathering processes and their relationship with catchment hydrology (Wohl et al., 2012; Floury et al., 2017).

Isotopic tracers that are sensitive to chemical weathering processes can be used to help understand the controls on concentration-discharge relationships. Many studies have highlighted the potential of lithium (Li) and magnesium (Mg) isotopes for characterising the variety of weathering processes that occur in the natural environment (Teng et al., 2010; Pogge von Strandmann et al., 2012; Tipper et al., 2012). These isotope systems provide insight as to plant uptake (Bolou-Bi et al., 2012) and sources of dissolved solutes (Kisakurek et al., 2005; Weynell et al., 2017), as well as the importance

of mineral (trans)formations (Ryu et al., 2014; Ma et al., 2015). Li and Mg isotopes are also fractionated during the formation of secondary minerals (Opfergelt et al., 2012; Henchiri et al., 2014; Trostle et al., 2014; Clergue et al., 2015; Dellinger et al., 2015; Dessert et al., 2015; Henchiri et al., 2016; Chapela Lara et al., 2017) and are thus well suited for tracing water-rock interactions in weathering systems. Here, we investigate the Li and Mg isotope composition of fluids from a small catchment in Guadeloupe (Quiock Creek) during a stormy period of one month. Throughfall, soil solution, river waters and groundwater were sampled to assess the effects of hydrological changes on Li and Mg isotopes.

2. Site description

Quiock Creek catchment (16°17'N, 61°70'W) is located on Basse-Terre Island, the volcanic part of the Guadeloupe archipelago in the French West Indies (Figure A1), and covers an area of ~8 hectares. The catchment is a Critical Zone Observatory (CZO), part of the Observatoire de l'Eau et de l'éRosion aux Antilles (ObsERA), which is operated by INSU-CNRS (OZCAR, the French National Research Infrastructure of CZOs) and the Institut de Physique du Globe de Paris (IPGP), and is devoted to the study of weathering and erosion of volcanic islands under tropical climate conditions. Quiock Creek is a small tributary of the Bras-David River, which is located in primary tropical rainforest in the Guadeloupe National Park. Rainfall variation is high in Basse-Terre and varies with the strength of the Northeast trade winds and topography. The mean annual temperature and throughfall rate (the quantity of rainfall that reaches the ground having passed through the subaerial vegetation) are, respectively, 25 °C and 3079 $mm.yr^{-1}$, and the rate of infiltration is relatively fast, ~0.1-1 $mm.s^{-1}$ (Guérin, 2015). Climate is characterised by two seasons: a dry season, from January to June, and a cyclonic wet season, from July to December. Wet seasons are associated with intense rainfall events initiated by tropical depressions and cyclones (Zahibo et al., 2007) that significantly contribute to the water budget. The rate of evapotranspiration is around 63% (Clergue et al., 2015). The mean hourly discharge ranges between 9.9 m^3/h and 10.3 m^3/h over the course of the year (Clergue et al., 2015; Guérin, 2015), which is five times lower than the Bras-David river (~50.4 m^3/h; Lloret et al., 2011). The subsurface of Quiock Creek catchment hosts an

unconfined aquifer (i.e. it is connected to the atmosphere) with a porosity of ~2% and a permeability of ~10^{-6} m/s (Guérin, 2015). During storm flow Quiock Creek discharge increases in proportion to the rainfall rate, whereas during drought flow the discharge decreases as a power law with time. This behaviour shows that the Quiock Creek aquifer acts as a non-linear filter between precipitation inputs and river discharge (Guérin, 2015), which suggests that Quiock Creek is mostly fed by groundwater. This is also supported by the fact that the creek flows throughout most of the year, even after long periods of drought (Guérin, 2015). In turn, the catchment is relatively unaffected by overland flow due to its smooth topography and the fast infiltration rate (Guérin, 2015).

Quiock Creek catchment is underlain by Pleistocene andesitic pyroclastic deposits that are usually covered by >15 meters of highly-weathered ferralitic regolith (Clergue et al., 2015). The deep regolith isolates groundwater and vegetation from the bedrock. The mineralogy, chemistry and resistivity of the regolith shows little variation with depth (Guérin, 2015). The bulk regolith is highly weathered and is composed of 95 wt.% of secondary mineral phases with clays (mostly halloysite and kaolinite) accounting for 70 wt.% of the secondary minerals; the remaining 30% mainly consists of Fe(III)-hydroxides and gibbsite (Buss et al., 2010). Primary minerals consist of quartz (0–8 wt%), feldspar (0–4 wt.%) and volcanic dust from Monserrat (~3 wt.%). The upper 30 cm of the profile is slightly enriched in quartz and feldspars (dominantly orthoclase) due to deposition of Saharan dust, the main terrestrial dust source to Guadeloupe (Buss et al., 2010; Clergue et al., 2015). The dust flux is highest between the months of June and October (Graham and Duce, 1979). The regolith is strongly depleted in soluble cations compared to the bedrock (Buss et al., 2010) and it supports a dense tropical rainforest that has a mean litter flux of 7.8 t ha^{-1} yr^{-1}.

3. **Methodology**

3.1 Sample collection and elemental analyses

A total of 55 water samples comprising throughfall, soil solution, river water and groundwater were collected in Quiock Creek catchment over a period of 21 days in October 2015 (Figure 1). Soil solution and groundwater reservoirs were emptied after sampling to remove the “stagnant” water

such that only “fresh” water was collected when they were next sampled. Soil solution reservoirs were emptied on 18/09/2015, 18 days before the first sampling date (Day 1, 06/10/2015), but the groundwater reservoirs were not emptied prior to the first sampling date. Temperature, conductivity and pH were directly measured in the field with a combined pH and conductivity probe (Hanna Instruments HI 98130; ± 0.5°C for temperature, ± 2% for conductivity, and ± 0.01 pH units for pH). Fluid samples were filtered at 0.2 µm-porosity through a cellulose acetate filter, and collected in 250 or 500 mL acid-cleaned HDPE bottles for cation analysis and in Milli-Q water (18.2 MΩ cm^{-1} H_2O) washed 30 mL bottles for anion analysis. The cation samples were acidified to pH ≈ 2 with distilled nitric acid. Alkalinity was determined by titration with 0.01 M HCl within 24 hours of sample collection.

Major and minor cation (Na, Ca, Mg, K, Al, B, Fe, Sr, Li) and silicon concentrations were measured by inductively-coupled plasma-source mass spectrometry (ICP-MS; Thermo X-Series II) at the National Oceanography Centre Southampton (NOCS). Analyses were calibrated using a set of synthetic multi-element standards prepared gravimetrically from high purity single element standard solutions. The certified standard reference material SLRS-6 (river water) and IAPSO seawater were analysed multiple times (n = 8) alongside the samples to assess the accuracy of the analyses, which was within ± 5% of the certified values. Anion (Cl and SO_4) concentrations were measured by ion chromatography (Dionex ICS2500) and calibrated using a set of synthetic multi-element standards prepared gravimetrically from high purity single element standard solutions. IAPSO seawater was analysed multiple times (n = 7) alongside the samples to assess the accuracy of the analyses, which was within ± 5% of the certified values.

3.2 Li and Mg isotope analyses

For Li isotope analysis, an aliquot of each water sample equivalent to 20 ng of Li was dried down and re-dissolved in 0.2 M HCl and loaded onto a cation exchange column filled with BioRad AG50W-X12 cation exchange resin to separate Li from the sample matrix (James and Palmer, 2000). Lithium isotope ratios were determined by multi-collector inductively-coupled plasma-source mass spectrometry (MC-ICP-MS; Thermo Scientific Neptune Plus) using a sample-standard bracketing

technique (Flesch et al., 1973), at NOCS. The Li isotope composition of samples is expressed as δ^7Li (‰), which is given by:

$$\delta\ ^7Li = \left[\frac{\left(\frac{^7Li}{^6Li}\right)_{sample}}{\left(\frac{^7Li}{^6Li}\right)_{L-SVEC}} - 1\right] \times 10^3 \qquad \textit{Eq. 1}$$

where L-SVEC is the Li isotope standard reference material (Flesch, 1973). The external reproducibility of the Li isotope analyses was assessed by repeated measurement of IAPSO seawater (δ^7Li = 30.9 ± 0.6‰; (2σ, n=27)), L-SVEC (δ^7Li = 0.0 ± 0.5‰ (2σ, n = 28)), and SLRS-6 river water (δ^7Li = 23.6 ± 0.7‰ (2σ, n = 3)).

For Mg isotope analysis, an aliquot of each water sample equivalent to 10 µg of Mg was dried down and re-dissolved in 0.8 M HNO_3 and loaded onto a cation exchange column filled with BioRad AG50W-X12 cation exchange resin to separate Mg from the sample matrix (Tipper et al., 2006b; Pogge von Strandmann, 2008). Magnesium isotope ratios were determined by MC-ICP-MS (Thermo Scientific Neptune Plus) using a sample-standard bracketing technique. The Mg isotope composition of samples is expressed as δ^xMg (where x is ^{25}Mg or ^{26}Mg), which is given by:

$$\delta\ ^xMg = \left[\frac{\left(\frac{^xMg}{^{24}Mg}\right)_{sample}}{\left(\frac{^xMg}{^{24}Mg}\right)_{DSM-3}} - 1\right] \times 10^3 \qquad \textit{Eq. 2}$$

where DSM-3 is the Mg isotope standard (Galy et al., 2001). The external reproducibility of the measurements was determined by repeated analysis of IAPSO seawater (δ^{26}Mg = -0.82 ± 0.05‰ (2σ, n = 18)), DSM-3 (δ^{26}Mg = 0.00 ± 0.07‰ (2σ, n = 27)), and SLRS-6 river water (δ^{26}Mg = -1.22 ± 0.03‰ (2σ, n = 5)).

3.3 Hydrological measurements

Precipitation, discharge and water table data for the 21-day sampling period are shown in Figure 2. Additional data, for the period between 18/09/2015 (when the soil solution reservoirs were first emptied) and 06/10/2015 are given in the Appendix (Figure A2). Rainfall was measured using a tipping-bucket rain gauge. Discharge was measured using a Venturi Flume (19 x 26.6 x 250 cm) together with a pressure sensor (CS451, Campbell Scientific) that measured the water height (or

stage) to a precision of ±0.5 mm (Guérin, 2015). Water table elevation is reported relative to the river elevation so a value of zero means that the water table is below the river elevation, but water is present. The water table elevation was determined with a pressure sensor (CS451, Campbell Scientific, precision ±5 mm) connected to a data logger (CR800, Campbell Scientific, resolution ±1 mm) placed approximatively 15 cm above the bottom of the piezometer.

4. **Results**

Sample terminology is described in Table 1.Temperature, pH, conductivity and alkalinity data are summarized in Table 2. Major and minor element and Total Dissolved Solids (TDS) concentrations are displayed in Table 3. Li and Mg isotope measurements are summarized in Table 4.

4.1 Hydrological data, in-situ measurements, alkalinity and TDS

Levels of discharge and precipitation in the catchment during the sampling campaign are shown in Figure 2. The year 2015 was drier than usual, with a mean throughfall input of ~2509 mm in 2015 compared to an average of 3079 mm/yr between 2011 and 2013 (Clergue et al., 2015). Similarly, the mean discharge in 2015 was ~5.2 m^3/h compared to ~10 m^3/h between 2011 and 2013. During the one-month period of this study, 283.6 mm of rain entered the catchment, corresponding to 12.5% of the total annual rain input in 2015. A series of large rain events occurred starting on days 4, 8, 11 and 19 of the sampling period (Figure 2). Three of these rain events noticeably increased the discharge in Quiock Creek (days 9, 11 and 19), and they also increased the elevation of the water table. Highest rainfall (92 mm) occurred on day 19, generating a peak discharge of 145 m^3/h. Because of previously dry conditions, the rainfall event on day 4 only triggered a small response in river discharge and water table (Figure 2).

The temperature of the river water samples ranged from 23.7 to 25.5°C, conductivity ranged from 35 to 56 µS/cm, pH ranged from 4.9 to 5.6, TDS concentrations ranged from 18 to 24 ppm and alkalinity was <10 µeq/L. All of these parameters showed a slight tendency to decrease with increasing discharge. Groundwater samples by comparison had generally higher pH (4.8 to 6.5), higher conductivity (48 to 109 µS/cm) and a wider range of alkalinity (5 to 1108 µeq/L) and TDS (21

to 97 ppm) values. Groundwaters collected from Piezo 2 had lower pH, conductivity and alkalinity compared to other groundwater samples. Groundwaters collected on Day 1 generally had higher alkalinities compared to samples collected later in the sampling campaign, presumably because the groundwater reservoir had not been emptied prior to sample collection, allowing greater time for water-rock reactions. The temperature of the groundwater samples (24.1 to 25.9°C) was close to that of the river water samples. The soil solutions were characterised by generally lower pH (4.5 to 5.5), TDS (15 to 25 ppm) and alkalinity (5 to 22 µeq/L) compared to the groundwater samples. The pH and conductivity of the throughfall samples were close to those of the soil solutions (respectively, 5.9 and 42 µS/cm), but the throughfall samples had higher alkalinity and lower TDS.

4.2 Composition of the dissolved load

The accuracy of the analyses for major ions can be estimated from the electrical balance (E.B., Eq. 3) of the cations and anions (expressed in meq/L):

$$\text{Electrical Balance (E.B., \%)} = \frac{\text{Sum cations} - \text{Sum anions}}{\text{Sum cations} + \text{Sum anions}} \times 100 \qquad \textit{Eq. 3}$$

The electrical balance was within ±10% and for most samples it was within ±5% (Figure A3). This indicates that there is no significant contribution to the geochemical composition of the waters from any species not reported in Table 3 (Appelo and Postma, 2004). Additionally, TDS extrapolated from conductivity measurements made in the field were well correlated with TDS measurements made in the laboratory indicating that the chemical composition of the samples was preserved between collection and analysis (Figure A3).

The major ion compositions of catchment waters are plotted in a Piper diagram (Piper, 1953) in Figure 3. The two throughfall samples were chloride and sodium rich, showing a strong seawater influence, but they had higher Ca and K concentrations (18 - 21 µmol/kg for Ca and 31 - 67 µmol/kg for K) compared to rain water (3 - 8 µmol/L for Ca and 3 - 5 µmol/L for K; Dessert et al., 2015). Soil solutions were also chloride and sodium rich and their alkalinity (up to 22 µeq/L) and Mg content (11 - 43 µmol/kg) were variable. Quiock Creek samples contained higher proportions of Na and Cl compared to throughfall samples, and their chemical composition showed little variation throughout the sampling campaign. Groundwater samples contained proportionally higher calcium

and alkalinity than the other water samples and tend to become more enriched in chloride and sodium with decreasing distance from the river. The compositions of all of the samples were similar to those measured in 2012-2013 (Clergue et al., 2015) with the exception of the alkalinities of the soil solutions and Quiock Creek samples, which had higher alkalinity in 2012-2013 (11 - 66 µeq/L). Concentrations of TDS, Si, Li and Mg in Quiock Creek are plotted versus discharge in Figure 4. Most of these variables showed a linear, slightly inverse relationship with discharge (Q), in a log-log plot indicating that there is a power-law relationship (e.g. for Si, [Si] = aQ^b, where a and b are constants and b is the power-law exponent) between concentration and discharge (Godsey et al., 2009). A slope of 0 would indicate that concentrations remain constant despite changes in discharge (so-called "chemostatic behaviour"; Godsey et al., 2009), whereas a slope of -1 indicates that solute concentration become more dilute as discharge increases (concentration scales as 1/Q). All concentration-discharge plots had a slope of slightly less than zero (between -0.09 and -0.03) suggesting that Quiock Creek behaves almost chemostatically for most of the major elements. However, Li and Mg had a weaker relationship with discharge (R^2=0.23 and 0.47, respectively; Figure 4), and showed chemostatic behaviour only at low discharge.

4.3 Sea salt contribution

The chemical composition of river water was determined by inputs from several sources, including sea salt and dust delivered in precipitation. The contribution from sea salts can be assessed through analysis of the Cl content, assuming that all of the Cl in the river water comes from sea salt (Stallard and Edmond, 1981), and that Cl shows conservative behaviour in the weathering system. Thus, for Li:

$$[Li]_{Sea} = \left(\frac{Li}{Cl}\right)_{Sea} \times [Cl]_X \qquad \textit{Eq. 4}$$

where $(Li/Cl)_{sea}$ = 0.05 (Dessert et al., 2015) and X is either the soil solution, groundwater, or river water. The fraction of Li derived from sea salt in the different fluid reservoirs is given in Table 5.

The sea salt contribution in throughfall was determined using the seawater Li/Na ratio and the sample Na concentration instead, because Cl was not determined for sample Th1 (Keene et al., 1986; Clergue et al., 2015). The majority of the Na, and most of the Mg, in all of the fluid reservoirs

(throughfall, soil solutions, groundwater and river water) has a marine origin, whereas Li was mainly provided by other sources.

4.4 Li and Mg, and their isotopes

4.4.1 [Li] and δ^7Li

The Li concentration and Li isotope composition of the water samples are plotted in Figure 5A. Different critical zone reservoirs had very different dissolved Li concentrations ([Li]) and δ^7Li values, and the overall range was, respectively, between 14 to 95 nmol/kg and 1.8 to 16.8‰. Throughfall contained relatively low [Li], averaging ~14 nmol/kg, and had δ^7Li values of ~13.3‰. By contrast, the soil solutions (taken on Day 1 and Day 18, before and after rain events) generally had the highest Li concentrations of all of the reservoirs (29 to 95 nmol/kg), and lowest δ^7Li values (1.8 to 10.4‰) (Figure 5A and Figure 6). Soil solution data were consistent with other measurements of soil solutions in Quiock Creek catchment ([Li] = 41-121 nmol/kg and δ^7Li = 4.6 to 8.9‰; Clergue et al., 2015). [Li] and δ^7Li were variable in the upper 300 cm of the soil profile, whereas [Li] increased with depth and δ^7Li decreased with depth in the deeper part of the profile (>300 cm). There was little difference in either the Li concentration or the δ^7Li value of soil solutions sampled before and after the rain events.

Groundwaters generally had highest δ^7Li values (up to 21‰), but they had generally lower [Li] than the soil solutions (29 to 92 nmol/kg; Figure 5A and Figure 7A). Significantly higher Li concentrations (~288 to 3026 nmol/L) were found in shallow and deep groundwater in the Columbia River Basalts (Liu et al., 2015). Lithium concentrations increased towards the river whereas δ^7Li values decreased from ~16‰ 30 m away from the river channel to ~9‰ close to the river (Figure 7B). The groundwater sample from Piezo 5 had much higher [Li] than the rest of the samples (92 nmol/kg compared to ~35 nmol/kg at the adjacent sampling site, Piezo 6), but its δ^7Li value was similar to samples recovered from Piezo 6. Whereas the Li concentrations in samples collected on different days were similar in all the piezometers, their δ^7Li values varied by up to 4‰ (e.g. Piezo 3 and 4). By contrast, all of the groundwater samples from Piezo 6 had very consistent Li concentrations (35 ± 5 nmol/kg; n = 3) and δ^7Li values (16.5 ± 0.3‰; n = 3).

The Li content of the river waters (~55 nmol/kg) was generally lower than the soil solutions, and was also relatively low compared to the world's major rivers ([Li] = ~215 nmol/L; Huh et al., 1998) but comparable to other rivers draining basaltic tropical catchments (Henchiri et al., 2014). δ^7Li values (7.2 to 10‰) were similar to those measured in a previous sampling campaign in Quiock Creek (δ^7Li = 8 to 9.3‰ (n = 4), (Clergue et al., 2015)) and other highly-weathered catchments (1-16‰; Dellinger et al., 2015 and references therein) and volcanic islands (e. g. Martinique δ^7Li = 4.9 to 20.6‰; Rad et al., 2013). However, Martinique rivers can be strongly affected by hydrothermal inputs (that have δ^7Li = ~1.6‰; Rad et al., 2013), whereas Quiock Creek is not affected by hydrothermal inputs (Clergue et al., 2015). Li concentrations tended to slightly decrease with increasing discharge (Figure 4) but there was no relationship between discharge and δ^7Li values (Figure A4). However, two samples (QC20 and QC21) measured during and a day after a storm event had relatively low [Li] and δ^7Li ([Li] = ~40 nmol/kg and δ^7Li = ~7.4‰).

4.4.2 [Mg] and δ^{26}Mg

The Mg concentration and Mg isotope composition of the catchment samples are plotted together in Figure 5B. The Mg concentrations of the two throughfall samples were similar (18 µmol/kg and 14 µmol/kg), but their corresponding δ^{26}Mg values were slightly different (-0.97 and -0.84‰; Figure 5B) but close to the value for seawater (-0.82 ± 0.05‰; Foster et al., 2010; Ryu et al., 2016). The δ^{26}Mg values of the throughfall samples are similar to values measured in rainwater in Guadeloupe (-0.87 ± 0.05‰ and -0.86 ± 0.11‰; Dessert et al., 2015), and in openfall precipitation in Puerto Rico (-1.10 to -0.92‰; Chapela Lara et al., 2017).

The concentration of Mg in the soil solutions (10 to 43 µmol/kg) was generally lower than the Mg concentration of throughfall, and the soil solutions generally have higher δ^{26}Mg (-1.04 to -0.58‰; Figure 5B and Figure 6) compared to other reservoirs. The Mg concentrations were within the range of those previously measured in Quiock Creek catchment (11-32 µmol/L; Clergue et al. (2015)), and in soil solutions from Puerto Rico (6 to 68 µmol/L; Chapela Lara et al., 2017). There was no clear trend between [Mg] and depth, but δ^{26}Mg values increased progressively from -1.04‰ at the surface to -0.65‰ at 1250 cm. This pattern of increasing soil solution δ^{26}Mg with depth has also been observed in soil profiles from California (from -0.99‰ at the surface to -0.43‰ at the base of

the profile; Tipper et al., 2010) and Puerto Rico (from -0.78‰ at the surface to -0.22‰ at the base of the profile; Chapela Lara et al., 2017). Soil solutions sampled on Day 18 have higher [Mg] in the upper part of the profile, compared to the samples measured on Day 1, whereas in the deeper part of the profile there was no obvious change in [Mg]. The δ^{26}Mg values of soil pore waters were generally identical within analytical uncertainty between Day 1 and Day 18.

Groundwaters sampled before and after significant rain events (Day 1 and 9) had the lowest δ^{26}Mg values (from -1.48 to -0.81‰) and the highest Mg concentrations (from 21 to 54 µmol/kg) compared to any of the other Quiock Creek fluids (Figure 5B and Figure 7C and D). The range of δ^{26}Mg measured in the groundwaters was comparable with other reported groundwaters (-1.70 to 0.23‰; (Teng, 2017). There was no obvious change in groundwater Mg concentration with distance from the river channel, but [Mg] decreased by 10-23 µmol/kg after the significant rain event on Day 9, reaching values similar to the throughfall concentration. Similarly, there was no obvious change in δ^{26}Mg with distance from the river channel (Figure 7D). However, three samples taken from piezometers 4 and 5 (Piezo 41, Piezo 49 and Piezo 51) had significantly lower δ^{26}Mg (-1.48 to -1.07‰) compared to any of the other samples. The Mg concentrations and δ^{26}Mg values of groundwaters from Piezo 6 (respectively, 21 to 27 µmol/kg and -0.99 to -0.95‰) were relatively stable throughout the sampling period but the δ^{26}Mg values of all of the other groundwater samples increased by 0.05 to 0.41‰ after the rainfall event, towards the value measured in throughfall.

Mg concentrations of samples from Quiock Creek ranged between 22 and 29 µmol/kg. δ^{26}Mg values showed a limited range, from -0.87 to -0.72‰, and there was no obvious relationship between either [Mg] or δ^{26}Mg with discharge (Figure 4 and Figure A4) even at very high discharge. These δ^{26}Mg values were lighter than those measured in other Guadeloupe rivers (-0.59 and -0.43‰; Dessert et al., 2015), but within the range measured in the world's largest rivers (-0.52 to -1.70‰; Tipper et al., 2006b), and rivers in Puerto Rico (-0.57 to 0.01‰), with the exception of one sample (δ^{26}Mg = -0.74‰) that was sampled when discharge was extremely high (Chapela Lara et al., 2017).

5. Discussion

5.1 Sources of Li and Mg in Quiock Creek catchment

The isotope compositions of Mg and Li are plotted with sea salt-corrected elemental ratios (Mg/Ca and Li/Na, respectively) in Figure 8 and Figure 9 to help characterize the possible sources of Mg and Li in the catchment. The use of elemental ratios allows for better comparison between the fluids as they are unaffected by dilution and evaporation processes (Gaillardet et al., 1999). Mg and Ca are both soluble alkaline earth elements that are susceptible to uptake by plants. However, in volcanic settings, Mg is more likely to be incorporated into secondary clays or adsorbed on clay mineral surfaces (Tipper et al., 2006a, 2008). Figure 8 shows that the Mg/Ca ratios of different reservoirs of Mg in the catchment can be very variable but the Mg isotope composition of the river waters and most of the groundwaters is within the range of throughfall and sea salt, consistent with the estimates of sea salt contribution reported in Table 5. However, groundwater samples from Piezo 41, Piezo 49 and Piezo 51 have much lower δ^{26}Mg that cannot be explained by mixing between any of the potential Mg reservoirs analysed in this study. We investigate the possible causes of these low δ^{26}Mg values in Section 5.3. Li and Na are both soluble alkali metals and are not essential nutrients, so they can be expected to act similarly during weathering. However, Na is generally not incorporated into secondary minerals whereas Li can be significantly enriched in clays and oxy-hydroxides (Sawhney, 1972; Millot et al., 2010; Dellinger et al., 2015). Figure 9 shows that most of the Quiock Creek fluids have Li/Na and δ^{7}Li values that are intermediate between sea salts that have low Li/Na and high δ^{7}Li, and Saharan dust or bulk soil that have much lower δ^{7}Li and higher Li/Na (Clergue et al., 2015). However, many of the samples have higher δ^{7}Li than predicted by simple binary mixing, which can likely be attributed to uptake of Li into secondary mineral phases (Huh et al., 1998; Huh et al., 2001; Rudnick et al., 2004; Kisakurek et al., 2005).

5.2 Controls on the Li and Mg isotope composition of throughfall and soil solutions

5.2.1 Li and Mg isotopes in throughfall

The δ^7Li values of the two throughfall samples (13 and 13.6‰) are much lower than that of sea salt (δ^7Li = ~31‰; Pogge von Strandmann et al. (2017)), suggesting that there is additional input of Li from a source with lower δ^7Li. The source of this Li is most likely to be leaching of Saharan dust located on the canopy, which has δ^7Li = -0.7‰ (Clergue et al., 2015). Assuming that no fractionation of Li isotopes occurs during dust dissolution (Pistiner and Henderson, 2003; Wimpenny et al., 2010), then mass balance considerations indicate that approximately 50% of the Li in throughfall comes from Saharan dust, consistent with estimations of the sea salt contribution (44-48% of Li was derived from sea salt; Table 5). Note, however, that this estimate is specific to our sampling period, as at other times of the year, the dust contribution to the Li load may be lower (as low as 25%; Clergue et al. (2015)).

The δ^{26}Mg values of the two throughfall samples differ by 0.13‰, just outside of the uncertainty of the analyses. This difference is unlikely to be due to differences in dust input, as no difference in δ^7Li is observed in the throughfall samples. The variation of δ^{26}Mg in the throughfall could be due to differences in inputs of Mg from the canopy. While plants are overall enriched in heavy Mg isotopes compared to the soil solution, the transfer of Mg from the roots to the leaves fractionates Mg isotopes, such that the upper part of the plant has lower δ^{26}Mg (Bolou-Bi et al., 2010; Bolou-Bi et al., 2012). Sample Th1 has lower δ^{26}Mg and higher [K] compared to sample Th3 (Table 3); high concentrations of K in rainfall and throughfall are indicative of input of K from vegetation (Riotte et al., 2014). By contrast, vegetation inputs have little effect on δ^7Li (Lemarchand et al., 2010; Clergue et al., 2015).

5.2.2 Li isotopes in the soil solution

Soil solution δ^7Li decreases with depth (from 10.4 to 1.8‰) and the δ^7Li value of bulk soil also decreases with depth (from 0.6 to -13.5‰; Clergue et al., 2015). The change in the δ^7Li value of the bulk soil has been attributed to increased dust input to the upper part of the soil profile (Clergue et

al., 2015). In the soil solutions, however, the proportion of Li derived from sea salt does not decrease significantly with depth (Figure A5), suggesting that changes in δ^7Li in the soil solution must be principally controlled by weathering processes rather than atmospheric inputs. However, in the upper part of the soil profile, the δ^7Li value of the soil solution increases after the rain events, whereas the Li/Na ratio decreases (Figure 6 and Figure A5). This is consistent with increased input of Li from throughfall that has relatively high δ^7Li and low Li/Na. Thus, the soil solution δ^7Li in the upper part of the profile appears to be much more influenced by throughfall inputs compared to the deeper part of the soil profile.

5.2.3 Mg isotopes in the soil solution

In contrast to Li, almost all of the Mg in the soil solution is delivered by atmospheric inputs (Table 5), which is consistent with the strong depletion of Mg in the soil of the catchment (Clergue et al., 2015). Nevertheless, the δ^{26}Mg values of the soil solutions increase slightly with depth in the soil profile; this cannot be attributed to simple mixing between throughfall and Mg derived from the bulk soil (Figure 8), suggesting that Mg isotope fractionation must occur during weathering. As all of the Cl in the soil solution comes from throughfall, and Cl is conservative during water transfer into the soil, changes in the Mg/Cl ratio of the soil solution can be used to identify whether the soils are a source or a sink of Mg. Therefore, the decrease of Mg/Cl suggests that Mg is removed from the soil solution in the deeper part of the soil profile, this removal leading to an increase in δ^{26}Mg (Figure A6).

Magnesium may also potentially be affected by vegetation uptake. The soil solutions have much lower K/Na than the throughfall (Figure A5), which is indicative of uptake of K (and by analogy uptake of Mg) by plants (Jobbagy and Jackson, 2001). However, this appears to have limited impact on the δ^{26}Mg value of the soil solutions, consistent with results from a previous study (Chapela Lara et al., 2017). Despite dense vegetation cover and tight nutrient cycles in tropical rainforests (Wood et al., 2009), the δ^{26}Mg of soil solutions therefore appears to be unaffected by plant uptake, most likely because atmospheric inputs of Mg are high there. This is a major difference with more temperate mountainous areas where lower δ^{26}Mg in soil water has been attributed to preferential uptake of the heavy Mg isotopes by plants (Uhlig et al., 2017).

The change in δ^{26}Mg must reflect preferential incorporation of light Mg isotopes into secondary mineral phases, or preferential adsorption of light Mg isotopes, in the deeper part of the soil profile. In Guadeloupe, soils tend to be enriched in heavy Mg isotopes compared to the fluids (Opfergelt et al., 2012; Dessert et al., 2015), which suggests that secondary minerals are enriched in heavy, not light, Mg isotopes. However, several studies have shown that cation exchange can lead to preferential uptake of light Mg isotopes onto mineral surfaces, increasing the δ^{26}Mg value of Mg that remains in solution (Jacobson et al., 2010; Opfergelt et al., 2012; Ma et al., 2015). Therefore, it seems likely that cation exchange occurs in the deepest part of the profile where the longer residence time of the water allows dissolved Mg to adsorb on the clay surfaces.

5.3 Weathering processes in groundwaters

The Li isotopic signature of groundwaters cannot be explained by simple mixing of Li from bulk soil or rock, and throughfall, as discussed in Section 5.1. The δ^{7}Li value of the groundwaters (8 to 16.8‰) is significantly higher than the δ^{7}Li value of the bulk soil (δ^{7}Li = 2.9‰ above 274 cm and -6.1‰ below 274 cm on average; Clergue et al., 2015) and, because primary minerals are almost totally absent from the soil (Buss et al., 2010), the δ^{7}Li value of the groundwaters must be linked to dissolution and precipitation of secondary mineral phases. After a rain event, the Li/Na ratio of the groundwaters increases, whereas the δ^{7}Li value of the groundwaters decreases (by 1.5 to 3.6‰ in Piezo 1, 2, 3 and 4; Figure 10). As this cannot only be attributed to input of Li from sea salt (Figure 9), implying that a ^{6}Li-enriched reservoir of Li in the catchment is contributing Li to groundwater during rain events, either through enhanced dissolution of secondary minerals - or through suppressed secondary mineral formation - during the time of the event itself, or through injection of previously isolated pockets of water enriched in ^{6}Li through interactions with secondary minerals before the rain event.

To further explore the possibility of a change in the rate of secondary mineral dissolution during a rain event, the saturation states of the groundwaters with respect to different secondary mineral phases were calculated with the PHREEQC program (Parkhurst and Appelo, 2013) using the measured concentration data, field pH and temperature. PHREEQC calculates mineral stability in

terms of the saturation index (SI). If SI > 0, the solution is supersaturated and the mineral may precipitate, whereas if SI < 0, the mineral is likely to dissolve. The groundwater SI for the principal constituents of the soil, kaolinite (halloysite), gibbsite and goethite (Buss et al., 2010), are shown in the Appendix (Figure A7). All of these mineral phases are oversaturated in the Quiock Creek groundwaters, so changes in δ^7Li are most likely controlled by changes in the rate of secondary mineral precipitation. After a rain event, the SI of all of the secondary mineral phases decreases, consistent with lower rates of secondary mineral precipitation and thus lower δ^7Li (Figure A7).

The majority of the groundwater samples have a Mg isotope composition similar to the groundwaters sampled in Piezo 6 (δ^{26}Mg = -0.95 to -0.99‰). The δ^{26}Mg value of these groundwaters was invariant over time, suggesting that they have a long residence time and that they represent the baseflow contribution to Quiock Creek. Two samples, Piezo 41 and Piezo 51, have significantly lower δ^{26}Mg values (respectively, -1.48 and -1.33‰). These samples contained 'stagnant' water, as the piezometers were not emptied prior to sampling (see Section 3.1). The low δ^{26}Mg values could be linked to: (1) release of Mg to groundwater from solid phases; (2) uptake or release of Mg by plants; or (3) cation exchange with mineral surfaces. Because soils and bedrock tend to be enriched in heavy Mg isotopes in Guadeloupe (Figure 8), addition of Mg with low δ^{26}Mg cannot be attributed to dissolution of mineral phases, dismissing hypothesis 1. In support of hypothesis 2 above, these two samples have much lower K/Cl and higher Mg/Cl and Mg/K ratios compared to the other groundwater samples (Figure 11). Potassium is an essential nutrient that is highly concentrated in plant tissues (Bowen, 1979; Riotte et al., 2014). The potential effects of vegetation on K and Mg in groundwaters include leaching of leaves that increases the K content of throughfall relative to sea salt and slightly decreases δ^{26}Mg due to preferential leaching of light Mg isotopes from the upper part of the plant (Bolou-Bi et al., 2010; Bolou-Bi et al., 2012); uptake of K, but not Mg, by plants; The two first patterns concur with analyses of soil solutions as discussed in Section 5.2.3, which suggests that groundwaters can be also affected by plant uptake. However, the lower K/Cl (Figure 11B) is inconsistent with reduced plant uptake which would have increased [K] relative to [Cl] (Jobbagy and Jackson, 2001). Therefore, it seems most likely that the low δ^{26}Mg groundwaters acquire Mg through cation exchange (hypothesis 3). As discussed in Section 5.2.3,

soil waters in the deeper part of the profile have relatively high $\delta^{26}Mg$ values, which is consistent with preferential adsorption of lighter Mg isotopes (Ma et al., 2015). Thus, desorption of this Mg can be expected to enrich groundwaters in light isotopes. These 'stagnant' groundwater samples have high [Ca]; Ca^{2+} has a higher ionic radius and a lower hydrated radius than Mg^{2+}, so it is preferentially adsorbed on clay surfaces (Udo, 1978; Appelo and Postma, 2004). As Ca^{2+} concentrations increase with increasing residence time, previously adsorbed light Mg isotopes are released in groundwater, increasing the Mg concentration and reducing the $\delta^{26}Mg$ value of the groundwater.

5.4 Temporal variations in the Mg and Li isotopic compositions of Quiock Creek waters

As the soils in Quiock Creek catchment are highly weathered, and as there is limited contact with the bedrock as the soils are thick, river waters can be expected to become more dilute during storm events. However, there was in fact little variation in element concentrations with discharge in this study, even though discharge varied by two orders of magnitude (Figure 4). At the highest discharge, [Li] and [Mg] were slightly lower (by ~25%) than expected for chemostatic behaviour, which implies that solute production is kinetically-limited at high discharge (Maher, 2011). This is consistent with the high permeability of the catchment (10^{-6}m/s or ~30m/yr; Guérin, 2015), which means that water residence time is relatively short.

In contrast to previous studies conducted in Guadeloupe and Puerto Rico (both tropical catchments), we find no evidence for increased river water $\delta^{26}Mg$ at low discharge, which has been attributed to an increased contribution of Mg from weathering from the deep saprolite at low flow (Dessert et al., 2015; Chapela Lara et al., 2017). This is likely related to the very high depletion of Mg and the absence of easily-weathered primary mineral phases in the soil (Buss et al., 2010). By contrast, the $\delta^{7}Li$ value of the river water decreased by, on average, ~2‰ after the largest rain event and remained low afterwards. The decrease in $\delta^{7}Li$ is most likely due to either input of Li from isolated pockets of soil solution with lower $\delta^{7}Li$ that are flushed out during rain events, or to a decrease in rates of secondary mineral precipitation during the rain event itself.

On a first order, the Li isotope composition of Quiock Creek (δ^7Li_{QC}) is controlled by mixing between Li derived from the soil solution and Li derived from groundwater:

$$\delta\,^7Li_{QC} = \delta\,^7Li_{Soil\ solution} \times f_{Soil\ solution} + \delta\,^7Li_{Groundwater} \times f_{Groundwater} \qquad \textit{Eq. 5}$$

$$f_{Soil\ solution} + f_{Groundwater} = 1 \qquad \textit{Eq. 6}$$

where $\delta^7Li_{Soil\ solution}$ and $\delta^7Li_{Groundwater}$ are the average isotope composition of the soil solution and groundwater respectively, and $f_{Soil\ solution}$ and $f_{Groundwater}$ represent, respectively, the flux of Li derived from the soil solution and groundwater. Hence:

$$f_{Soil\ solution} = \frac{\delta\,^7Li_{QC} - \delta\,^7Li_{Groundwater}}{\delta\,^7Li_{Soil\ solution} - \delta\,^7Li_{Groundwater}} \qquad \textit{Eq. 7}$$

Assuming that $\delta^7Li_{Soil\ solution}$ = 6.9 ± 2.6‰ and $\delta^7Li_{Groundwater}$ = 13.2 ± 3.2‰, we calculate that 52 to 73% of the Li in Quiock Creek came from the soil solution before the storm, whereas after the storm this increased to 89 to 95%. Thus, the decrease in δ^7Li was most likely due to increased input of Li from soil solution that has lower δ^7Li and was flushed out during the rain event.

The response of other elements, for which isotope data are not available, to the storm event can also be assessed if the ratio of the concentration of that element, normalised to a conservative element (e.g., Cl), differs between the different weathering reservoirs. This is not the case for most of the elements analysed in this study, with the exception of Ca. Groundwaters have an average molar Ca/Cl ratio of 697 ± 535, whereas soil solutions have Ca/Cl = 11 ± 8. We calculate that 96 ± 19% of the Ca in Quiock Creek came from soil solution before the storm event, and this did not change after the storm event (95 ± 21%). Thus, as for Li, soil solutions are an important source of Ca in Quiock Creek water.

6. Conclusions

This study highlights that, even in a highly-weathered catchment that drains single lithology, there can be significant differences in the Li and Mg isotope compositions of different critical zone reservoirs. Isotope signals are strongly affected by atmospheric inputs of Mg and Li, but they are also controlled by interactions with soil and bedrock. Li isotope compositions are mostly influenced by preferential incorporation of ^6Li into secondary minerals, whereas Mg isotope compositions

mainly reflect input of Mg from sea salts although adsorption or desorption of light Mg isotopes to/from mineral surfaces can occur in waters that have a relatively long residence time. δ^7Li values of groundwaters can quickly decrease even after a single rain event and this is likely due to lower rates of precipitation of secondary minerals. A rapid decrease in δ^7Li in Quiock Creek after a storm event is attributed to increased input of Li from soil solutions that have lower δ^7Li compared to groundwater. Atmospheric inputs of Li increase the δ^7Li of soil solutions after rain events only in the upper part of the soil profile. δ^{26}Mg values show little change during hydrological events, because most of the Mg in Quiock Creek catchment is supplied by throughfall and Mg is not significantly impacted by plant uptake.

Acknowledgements

This work would not have been achieved without logistical support from two INSU-CNRS observatories run by the IPGP: the Observatoire Volcanologique et Sismologique de Guadeloupe (OVSG) and the Observatoire de l'Eau et de l'Erosion aux Antilles (ObsErA, OZCAR Research Infrastructure). We are deeply grateful to the ObsErA advisor Eric Lajeunesse for sharing hydrological data. We thank in particular Vincent Robert from IPGP-OVSG and Guillaume Roehm for their assistance in field work. Matthew Cooper and Andy Milton (University of Southampton) are thanked for their help in performing the ICP-MS and MC-ICP-MS measurements. We gratefully acknowledge Edward Tipper and Martin Palmer for their helpful and critical comments on the original version of this paper. The research leading to these results has received funding from the People Programme (Marie Curie Actions) of the European Union's Seventh Framework Programme FP7/2007-2013/ under REA grant agreement n° [608069].

References

Appelo, C.A.J. and Postma, D. (2004) Geochemistry, groundwater and pollution. CRC press.

Benettin, P., Soulsby, C., Birkel, C., Tetzlaff, D., Botter, G. and Rinaldo, A. (2017) Using SAS functions and high-resolution isotope data to unravel travel time distributions in headwater catchments. Water Resources Research 53, 1864-1878.

Bolou-Bi, E.B., Poszwa, A., Leyval, C. and Vigier, N. (2010) Experimental determination of magnesium isotope fractionation during higher plant growth. Geochim. Cosmochim. Acta 74, 2523-2537.

Bolou-Bi, E.B., Vigier, N., Poszwa, A., Boudot, J.P. and Dambrine, E. (2012) Effects of biogeochemical processes on magnesium isotope variations in a forested catchment in the Vosges Mountains (France). Geochim. Cosmochim. Acta 87, 341-355.

Bouchez, J., Moquet, J.S., Espinoza, J.C., Martinez, J.M., Guyot, J.L., Lagane, C., Filizola, N., Noriega, L., Hidalgo Sanchez, L. and Pombosa, R. (2017) River mixing in the Amazon as a driver of concentration-discharge relationships. Water Resources Research 53, 8660-8685.

Bowen, H.J.M. (1979) Environmental chemistry of the elements. Academic Press, London, UK.

Buss, H., White, A., Dessert, C., Gaillardet, J., Blum, A. and Sak, P. (2010) Depth profiles in a tropical volcanic critical zone observatory: Basse-Terre, Guadeloupe, in: Torres-Alvarado, I.S., Birkkle, P. (Ed.), Proceedings of the 13th International Conference on Water–Rock Interaction. Taylor & Francis Group, London, UK.

Calmels, D., Galy, A., Hovius, N., Bickle, M., West, A.J., Chen, M.-C. and Chapman, H. (2011) Contribution of deep groundwater to the weathering budget in a rapidly eroding mountain belt, Taiwan. Earth Planet. Sci. Lett. 303, 48-58.

Chapela Lara, M., Buss, H.L., Pogge von Strandmann, P.A.E., Schuessler, J.A. and Moore, O.W. (2017) The influence of critical zone processes on the Mg isotope budget in a tropical, highly weathered andesitic catchment. Geochim. Cosmochim. Acta 202, 77-100.

Clergue, C., Dellinger, M., Buss, H.L., Gaillardet, J., Benedetti, M.F. and Dessert, C. (2015) Influence of atmospheric deposits and secondary minerals on Li isotopes budget in a highly weathered catchment, Guadeloupe (Lesser Antilles). Chem. Geol. 414, 28-41.

Clow, D.W. and Mast, M.A. (2010) Mechanisms for chemostatic behavior in catchments: Implications for CO_2 consumption by mineral weathering. Chem. Geol. 269, 40-51.

Colmeet-Daage, F. and Bernard, Z. (1979) Contribution à l'Atlas des départements d'Outre-mer : Guadeloupe. Carte des sols de la Guadeloupe, Grande-Terre, Marie-Galante. Carte des pentes et du modelé de la Guadeloupe, Grande-Terre, Marie-Galante. ORSTOM, Antilles.

Dellinger, M., Gaillardet, J., Bouchez, J., Calmels, D., Louvat, P., Dosseto, A., Gorge, C., Alanoca, L. and Maurice, L. (2015) Riverine Li isotope fractionation in the Amazon river basin controlled by the weathering regimes. Geochim. Cosmochim. Acta 164, 71-93.

Dessert, C., Lajeunesse, E., Lloret, E., Clergue, C., Crispi, O., Gorge, C. and Quidelleur, X. (2015) Controls on chemical weathering on a mountainous volcanic tropical island: Guadeloupe (French West Indies). Geochim. Cosmochim. Acta 171, 216-237.

Flesch, G., Anderson, A. and Svec, H. (1973) A secondary isotopic standard for $^{6}Li/^{7}Li$ determinations. Int. J. Mass Spectrom. Ion Phys. 12, 265-272.

Floury, P., Gaillardet, J., Gayer, E., Bouchez, J., Tallec, G., Ansart, P., Koch, F., Gorge, C., Blanchouin, A. and Roubaty, J.-L. (2017) The potamochemical symphony: new progress in the high-frequency acquisition of stream chemical data. Hydrol Earth Syst Sc 21, 6153.

Foster, G.L., Pogge von Strandmann, P.A.E. and Rae, J.W.B. (2010) Boron and magnesium isotopic composition of seawater. Geochem. Geophys. Geosyst. 11.

Gaillardet, J., Dupré, B., Louvat, P. and Allègre, C.J. (1999) Global silicate weathering and CO_2 consumption rates deduced from the chemistry of large rivers. Chem. Geol. 159, 3-30.

Galy, A., Belshaw, N.S., Halicz, L. and O'Nions, R.K. (2001) High-precision measurement of magnesium isotopes by multiple-collector inductively coupled plasma mass spectrometry. Int. J. Mass Spectrom. 208, 89-98.

Godsey, S.E., Kirchner, J.W. and Clow, D.W. (2009) Concentration-discharge relationships reflect chemostatic characteristics of US catchments. Hydrol. Processes 23, 1844-1864.

Graham, W.F. and Duce, R.A. (1979) Atmospheric pathways of the phosphorus cycle. Geochim. Cosmochim. Acta 43, 1195-1208.

Guérin, A. (2015) Dynamique de l’écoulement dans un aquifère non confiné. Université Paris Diderot (Doctoral dissertation).

Henchiri, S., Clergue, C., Dellinger, M., Gaillardet, J., Louvat, P. and Bouchez, J. (2014) The influence of hydrothermal activity on the Li isotopic signature of rivers draining volcanic areas. Geochemistry of the Earth's Surface Ges-10 10, 223-230.

Henchiri, S., Gaillardet, J., Dellinger, M., Bouchez, J. and Spencer, R.G.M. (2016) Riverine dissolved lithium isotopic signatures in low-relief central Africa and their link to weathering regimes. Geophys. Res. Lett. 43, 4391-4399.

Huh, Y., Chan, L.H., Zhang, L. and Edmond, J.M. (1998) Lithium and its isotopes in major world rivers: implications for weathering and the oceanic budget. Geochim. Cosmochim. Acta 62, 2039-2051.

Huh, Y., Chan, L.H. and Edmond, J.M. (2001) Lithium isotopes as a probe of weathering processes: Orinoco River. Earth Planet. Sci. Lett. 194, 189-199.

Jacobson, A.D., Zhang, Z.F., Lundstrom, C. and Huang, F. (2010) Behavior of Mg isotopes during dedolomitization in the Madison Aquifer, South Dakota. Earth Planet. Sci. Lett. 297, 446-452.

James, R.H. and Palmer, M.R. (2000) The lithium isotope composition of international rock standards. Chem. Geol. 166, 319-326.

Jobbagy, E.G. and Jackson, R.B. (2001) The distribution of soil nutrients with depth: global patterns and the imprint of plants. Biogeochemistry 53, 51-77.

Keene, W.C., Pszenny, A.A.P., Galloway, J.N. and Hawley, M.E. (1986) Sea-salt corrections and interpretation of constituent ratios in marine precipitation. J Geophys Res-Atmos 91, 6647-6658.

Kisakurek, B., James, R.H. and Harris, N.B.W. (2005) Li and δ^7Li in Himalayan rivers: proxies for silicate weathering? Earth Planet. Sci. Lett. 237, 387-401.

Larsen, M.C. and Simon, A. (1993) A rainfall intensity-duration threshold for landslides in a humid-tropical environment, Puerto Rico. Geografiska Annaler. Series A, Physical Geography 75, 13-23.

Lemarchand, E., Chabaux, F., Vigier, N., Millot, R. and Pierret, M.C. (2010) Lithium isotope systematics in a forested granitic catchment (Strengbach, Vosges Mountains, France). Geochim. Cosmochim. Acta 74, 4612-4628.

Liu, X.-M., Wanner, C., Rudnick, R.L. and McDonough, W.F. (2015) Processes controlling δ^7Li in rivers illuminated by study of streams and groundwaters draining basalts. Earth Planet. Sci. Lett. 409, 212-224.

Lloret, E. (2010) Dynamique du carbone dans des petits bassins versants tropicaux, Exemple de la Guadeloupe PhD Thesis Université Paris Diderot.

Lloret, E., Dessert, C., Gaillardet, J., Alberic, P., Crispi, O., Chaduteau, C. and Benedetti, M.F. (2011) Comparison of dissolved inorganic and organic carbon yields and fluxes in the watersheds of tropical volcanic islands, examples from Guadeloupe (French West Indies). Chem. Geol. 280, 65-78.

Ma, L., Teng, F.-Z., Jin, L., Ke, S., Yang, W., Gu, H.-O. and Brantley, S.L. (2015) Magnesium isotope fractionation during shale weathering in the Shale Hills critical zone observatory: accumulation of light Mg isotopes in soils by clay mineral transformation. Chem. Geol. 397, 37-50.

Maher, K. (2011) The role of fluid residence time and topographic scales in determining chemical fluxes from landscapes. Earth Planet. Sci. Lett. 312, 48-58.

Millot, R., Gaillardet, J., Dupre, B. and Allegre, C.J. (2002) The global control of silicate weathering rates and the coupling with physical erosion: new insights from rivers of the Canadian Shield. Earth Planet. Sci. Lett. 196, 83-98.

Millot, R., Vigier, N. and Gaillardet, J. (2010) Behaviour of lithium and its isotopes during weathering in the Mackenzie Basin, Canada. Geochim. Cosmochim. Acta 74, 3897-3912.

Opfergelt, S., Georg, R.B., Delvaux, B., Cabidoche, Y.M., Burton, K.W. and Halliday, A.N. (2012) Mechanisms of magnesium isotope fractionation in volcanic soil weathering sequences, Guadeloupe. Earth Planet. Sci. Lett. 341, 176-185.

Parkhurst, D.L. and Appelo, C.A.J. (2013) Description of input and examples for PHREEQC version 3-a computer program for speciation, batch-reaction, one-dimensional transport, and inverse geochemical calculations,U.S. Geological Survey Techniques and Methods, book 6, chap. A43, 497p., available only at http://pubs.usgs.gov/tm/06/a43.

Piper, A. (1953) A graphic procedure in the geochemical interpretation of water analysis, US department of the interior, geological survey. Water Resources Division, Ground Water Branch, Washington.

Pistiner, J.S. and Henderson, G.M. (2003) Lithium-isotope fractionation during continental weathering processes. Earth Planet. Sci. Lett. 214, 327-339.

Pogge von Strandmann, P.A.E. (2008) Precise magnesium isotope measurements in core top planktic and benthic foraminifera. Geochem. Geophys. Geosyst. 9.

Pogge von Strandmann, P.A.E., Opfergelt, S., Lai, Y.J., Sigfusson, B., Gislason, S.R. and Burton, K.W. (2012) Lithium, magnesium and silicon isotope behaviour accompanying weathering in a basaltic soil and pore water profile in Iceland. Earth Planet. Sci. Lett. 339, 11-23.

Pogge von Strandmann, P.A.E., Vaks, A., Bar-Matthews, M., Ayalon, A., Jacob, E. and Henderson, G.M. (2017) Lithium isotopes in speleothems: temperature-controlled variation in silicate weathering during glacial cycles. Earth Planet. Sci. Lett. 469, 64-74.

Rad, S., Rivé, K., Vittecoq, B., Cerdan, O. and Allègre, C.J. (2013) Chemical weathering and erosion rates in the Lesser Antilles: an overview in Guadeloupe, Martinique and Dominica. Journal of South American Earth Sciences 45, 331-344.

Riotte, J., Marechal, J.C., Audry, S., Kumar, C., Bedimo, J.P.B., Ruiz, L., Sekhar, M., Cisel, M., Tarak, R.C., Varma, M.R.R., Lagane, C., Reddy, P. and Braun, J.J. (2014) Vegetation impact on stream chemical fluxes: Mule Hole watershed (South India). Geochim. Cosmochim. Acta 145, 116-138.

Rudnick, R.L., Tomascak, P.B., Njo, H.B. and Gardner, L.R. (2004) Extreme lithium isotopic fractionation during continental weathering revealed in saprolites from South Carolina. Chem. Geol. 212, 45-57.

Ryu, J.-S., Vigier, N., Lee, S.-W., Lee, K.-S. and Chadwick, O.A. (2014) Variation of lithium isotope geochemistry during basalt weathering and secondary mineral transformations in Hawaii. Geochim. Cosmochim. Acta 145, 103-115.

Ryu, J.-S., Vigier, N., Decarreau, A., Lee, S.-W., Lee, K.-S., Song, H. and Petit, S. (2016) Experimental investigation of Mg isotope fractionation during mineral dissolution and clay formation. Chem. Geol. 445, 135-145.

Sawhney, B. (1972) Selective sorption and fixation of cations by clay minerals: A review. Clays Clay Miner. 20, 93-100.

Stallard, R.F. and Edmond, J.M. (1981) Geochemistry of the Amazon. 1. Precipitation chemistry and the marine contribution to the dissolved load at the time of peak discharge. J Geophys Res-Oceans 86, 9844-9858.

Teng, F.Z., Li, W.Y., Rudnick, R.L. and Gardner, L.R. (2010) Contrasting lithium and magnesium isotope fractionation during continental weathering. Earth Planet. Sci. Lett. 300, 63-71.

Teng, F.Z. (2017) Magnesium Isotope Geochemistry. Non-Traditional Stable Isotopes 82, 219-287.

Tipper, E.T., Galy, A. and Bickle, M.J. (2006a) Riverine evidence for a fractionated reservoir of Ca and Mg on the continents: Implications for the oceanic Ca cycle. Earth Planet. Sci. Lett. 247, 267-279.

Tipper, E.T., Galy, A., Gaillardet, J., Bickle, M.J., Elderfield, H. and Carder, E.A. (2006b) The magnesium isotope budget of the modem ocean: constraints from riverine magnesium isotope ratios. Earth Planet. Sci. Lett. 250, 241-253.

Tipper, E.T., Galy, A. and Bickle, M.J. (2008) Calcium and magnesium isotope systematics in rivers draining the Himalaya-Tibetan-Plateau region: lithological or fractionation control? Geochim. Cosmochim. Acta 72, 1057-1075.

Tipper, E.T., Gaillardet, J., Louvat, P., Capmas, F. and White, A.F. (2010) Mg isotope constraints on soil pore-fluid chemistry: evidence from Santa Cruz, California. Geochim. Cosmochim. Acta 74, 3883-3896.

Tipper, E.T., Calmels, D., Gaillardet, J., Louvat, P., Capmas, F. and Dubacq, B. (2012) Positive correlation between Li and Mg isotope ratios in the river waters of the Mackenzie Basin challenges the interpretation of apparent isotopic fractionation during weathering. Earth Planet. Sci. Lett. 333, 35-45.

Trostle, K., Derry, L., Vigier, N. and Chadwick, O. (2014) Magnesium isotope fractionation during arid pedogenesis on the island of Hawaii (USA). Procedia Earth Planet. Sci. 10, 243-248.

Udo, E.J. (1978) Thermodynamics of potassium-calcium and magnesium-calcium exchange-reactions on a kaolinitic soil clay. Soil Sci. Soc. Am. J. 42, 556-560.

Uhlig, D., Schuessler, J.A., Bouchez, J., Dixon, J.L. and von Blanckenburg, F. (2017) Quantifying nutrient uptake as driver of rock weathering in forest ecosystems by magnesium stable isotopes. Biogeosciences 14, 3111.

Weynell, M., Wiechert, U. and Schuessler, J.A. (2017) Lithium isotopes and implications on chemical weathering in the catchment of Lake Donggi Cona, northeastern Tibetan Plateau. Geochim. Cosmochim. Acta 213, 155-177.

Wimpenny, J., Gislason, S.R., James, R.H., Gannoun, A., Pogge Von Strandmann, P.A.E. and Burton, K.W. (2010) The behaviour of Li and Mg isotopes during primary phase dissolution and secondary mineral formation in basalt. Geochim. Cosmochim. Acta 74, 5259-5279.

Wohl, E., Barros, A., Brunsell, N., Chappell, N.A., Coe, M., Giambelluca, T., Goldsmith, S., Harmon, R., Hendrickx, J.M.H., Juvik, J., McDonnell, J. and Ogden, F. (2012) The hydrology of the humid tropics. Nat. Clim. Change 2, 655-662.

Wood, T.E., Lawrence, D., Clark, D.A. and Chazdon, R.L. (2009) Rain forest nutrient cycling and productivity in response to large-scale litter manipulation. Ecology 90, 109-121.

Zahibo, N., Pelinovsky, E., Talipova, T., Rabinovich, A., Kurkin, A. and Nikolkina, I. (2007) Statistical analysis of cyclone hazard for Guadeloupe, Lesser Antilles. Atmos. Res. 84, 13-29.

The response of Li and Mg isotopes to rain events in a highly-weathered catchment

David M. Fries[1], Rachael H. James[1], Céline Dessert[2], Julien Bouchez[2], Aurélien Beaumais[1, 3], Christopher R. Pearce[4]

[1]School of Ocean and Earth Science, National Oceanography Centre Southampton, University of Southampton Waterfront Campus, European Way, Southampton SO14 3ZH, UK

[2]Institut de Physique du Globe de Paris (IPGP), Sorbonne Paris Cité, Université Paris Diderot, CNRS, Paris, France

[3]DEN – Service d'Etudes Analytiques et de Réactivité des Surfaces (SEARS), CEA, Université Paris-Saclay, F-91191 Gif sur Yvette, France

[4]Marine Geoscience, National Oceanography Centre, Southampton SO14 3ZH, UK

Manuscript Figures 1-11

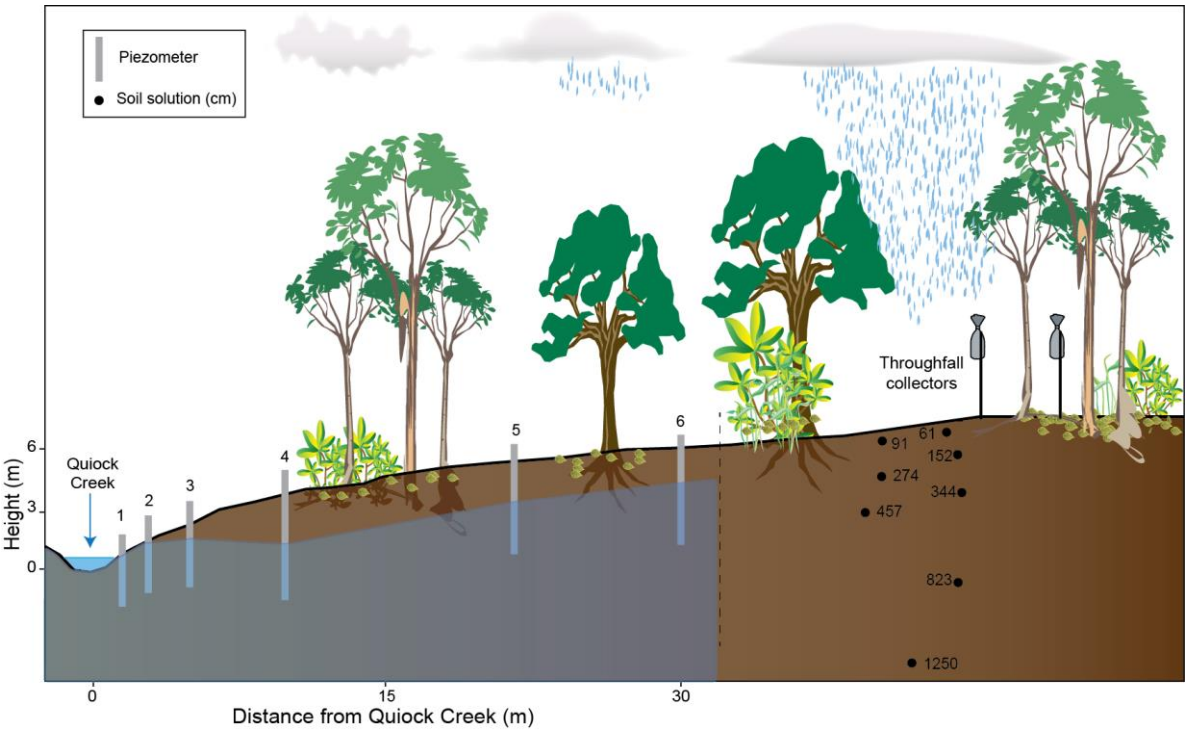

Figure 1. Schematic diagram showing the samples collected in Quiock Creek catchment. Depth of soil solution samples are shown as centimetres below the soil surface.

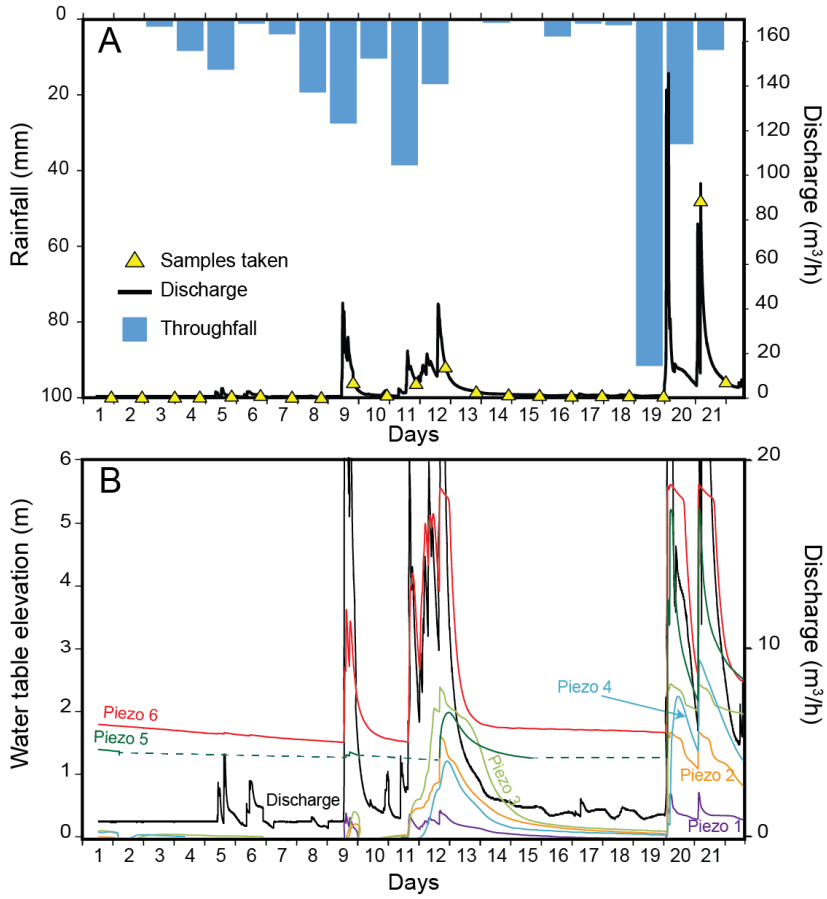

Figure 2. A. Precipitation and discharge of Quiock Creek. B. Water table elevation and discharge during the period of study. Data are from the ObsERA website (http://webobsera.ipgp.fr/).

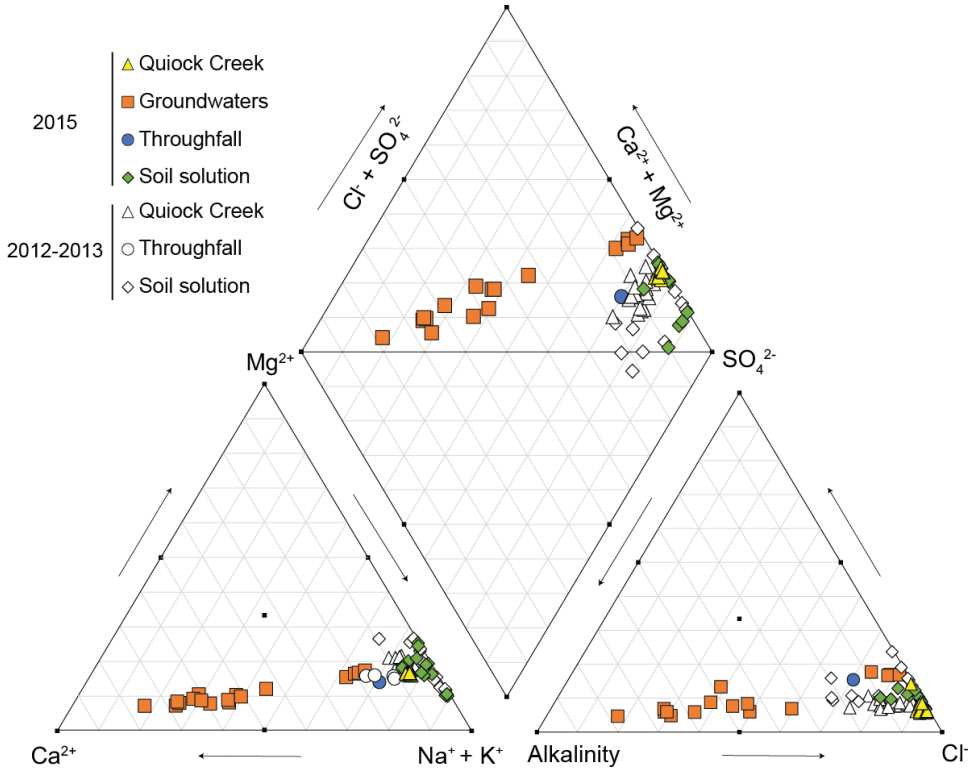

Figure 3. Piper diagram showing the relative abundance of anions and cations in samples from Quiock Creek catchment. Data for water samples collected in 2012-2013 (white symbols) are from Clergue et al. (2015).

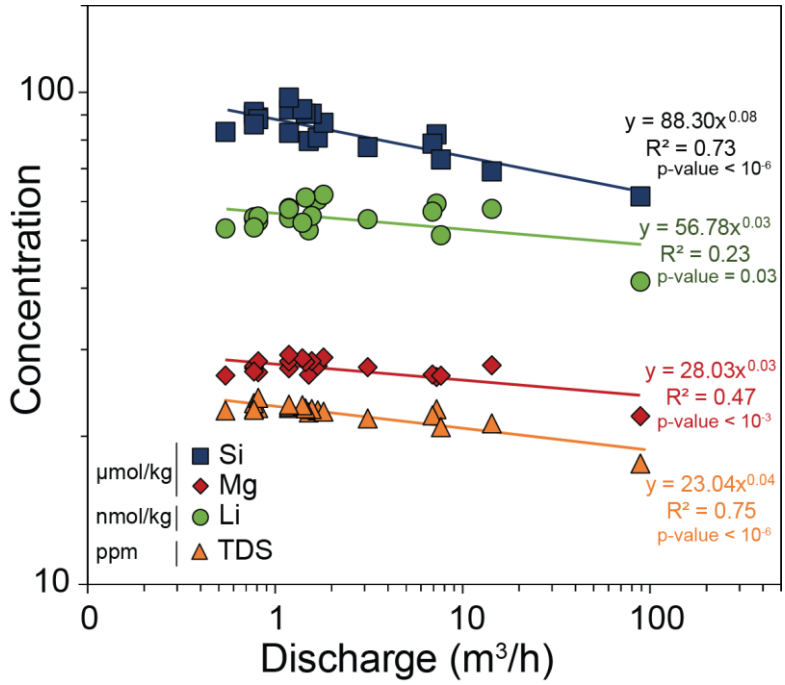

Figure 4. Si, Total Dissolved Solid (TDS), Mg and Li concentration in Quiock Creek as a function of discharge. Each coloured lines represents the power-law relationship between concentration and discharge.

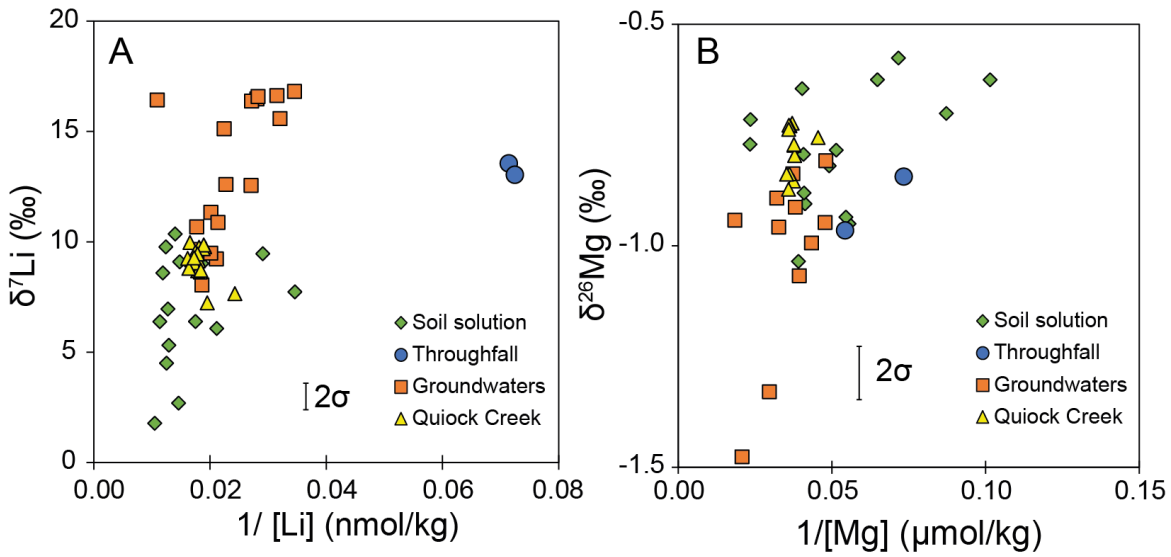

Figure 5. A. [Li] and δ^{7}Li values of the dissolved load in Quiock Creek catchment. B. [Mg] and δ^{26}Mg values of the dissolved load in Quiock Creek catchment. The error bars represent the external error (2σ) of the isotopic compositions. The external error on the Li and Mg concentration are smaller than the symbols.

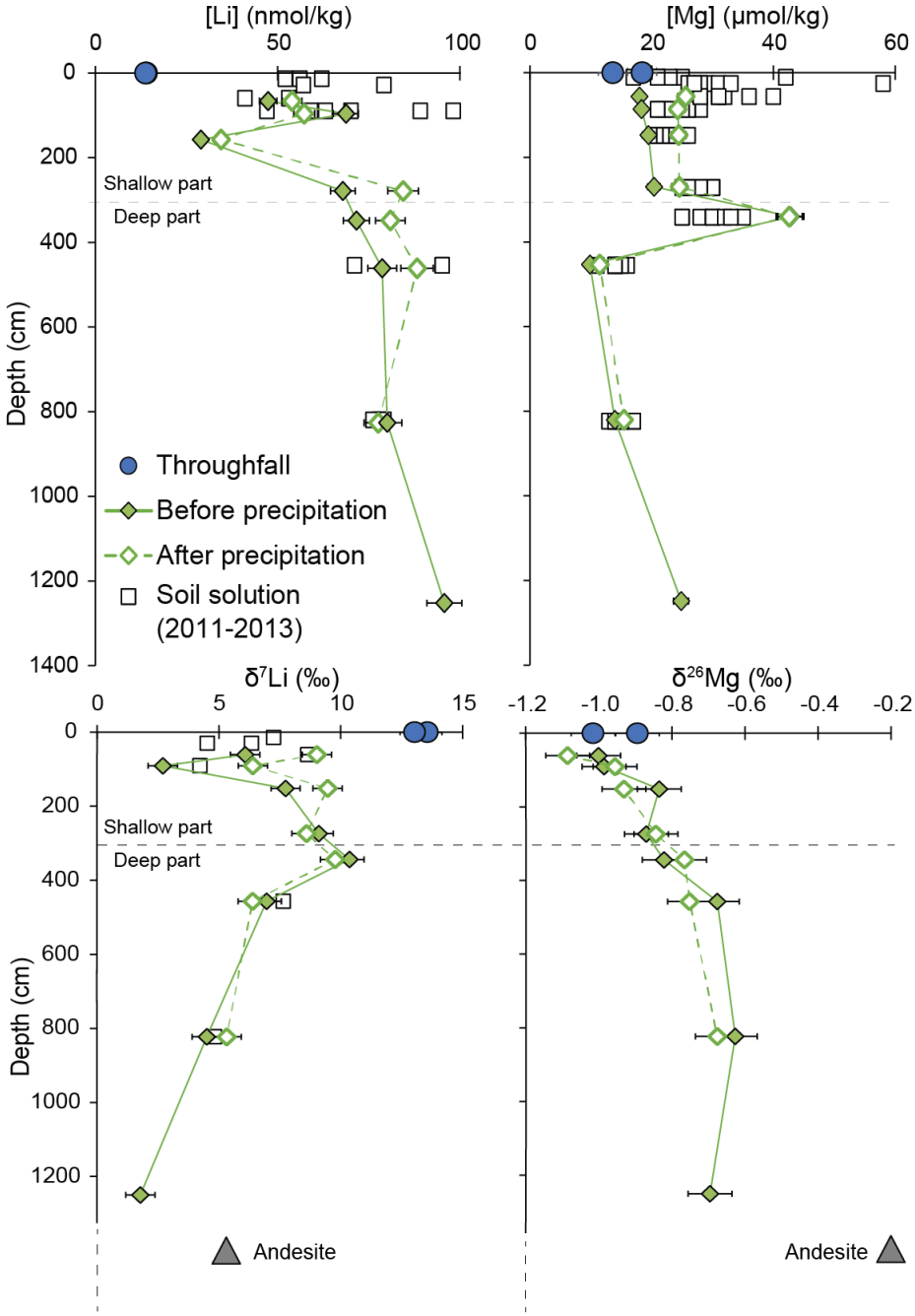

Figure 6. Li and Mg concentrations (± 5%) and isotope compositions of soil solutions taken before (Day 1) and after (Day 18) several rain events. Data for soil solution (collected in 2011-2013) are from Clergue et al. (2015), δ^{7}Li and δ^{26}Mg values for andesite are from Clergue et al. (2015) and Dessert et al. (2015).

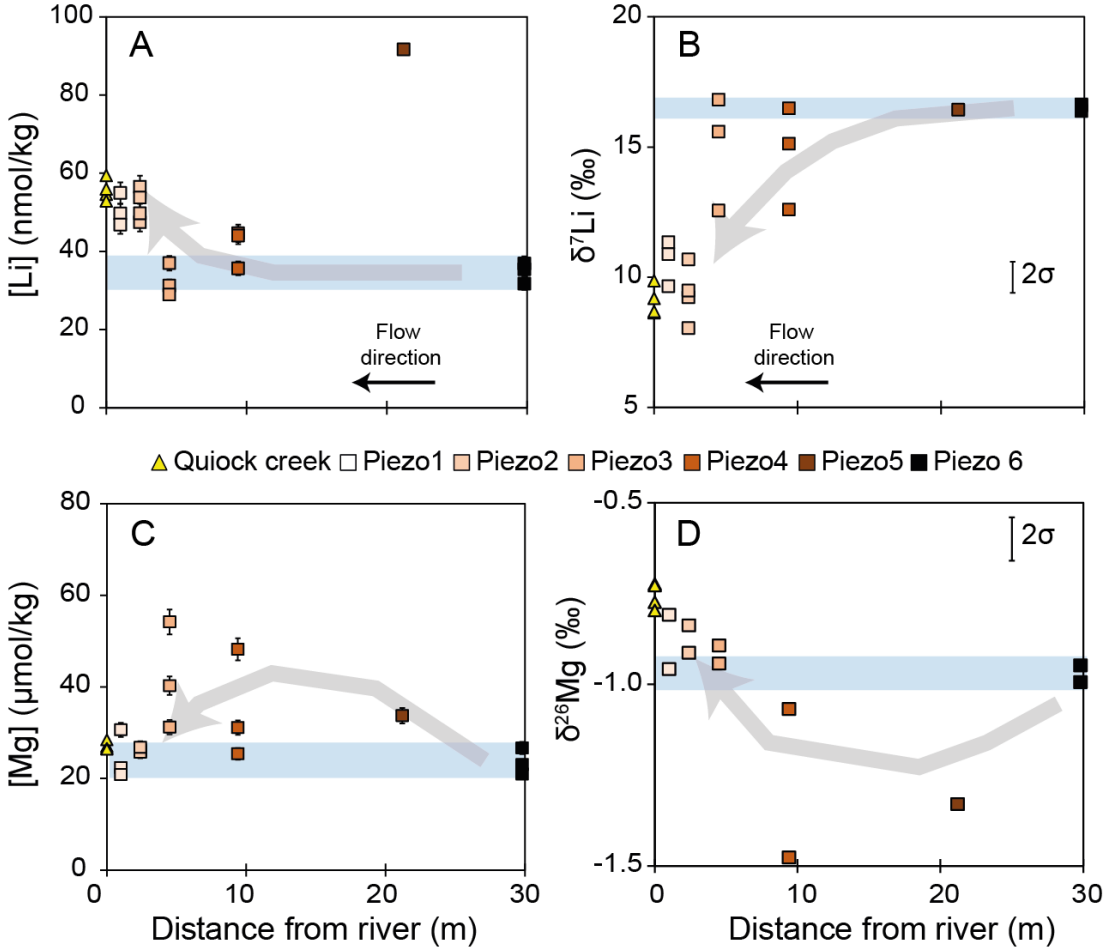

Figure 7. Evolution of groundwater [Li] and [Mg] (± 5%), δ^{7}Li and δ^{26}Mg versus distance to the river. Along this specific profile, groundwater from the Quiock Creek aquifer feeds Quiock Creek (Guérin, 2015). The blue shaded boxes highlight Piezo 6 samples likely represent river baseflow (see section 4.4.1). The grey shaded arrows show the general trend of the data points. Error bars show the external reproducibility of the isotope analyses (2σ).

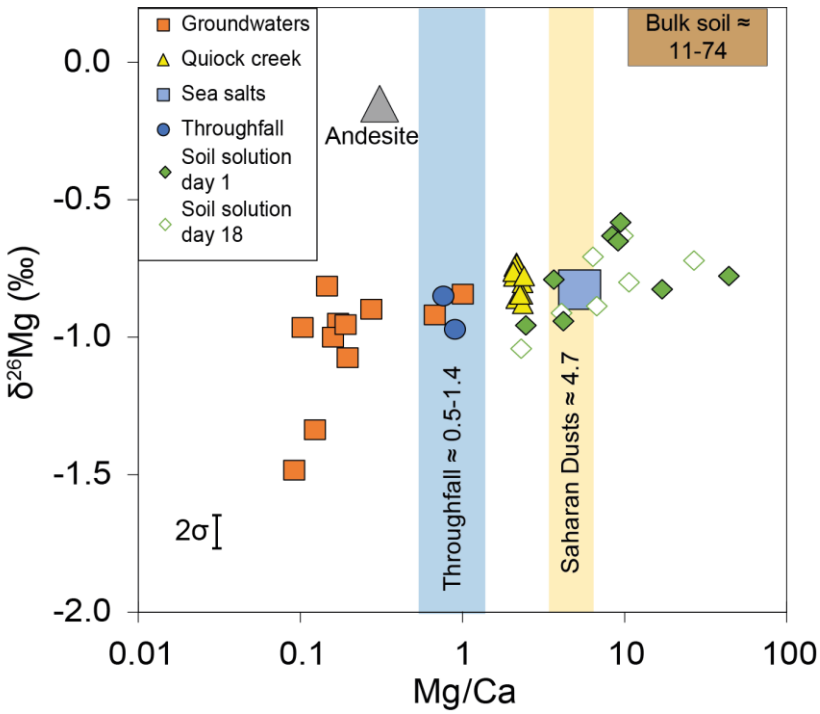

Figure 8. δ^{26}Mg versus Mg/Ca for fluids in Quiock Creek catchment. Bedrock (andesite) and bulk soil δ^{26}Mg are from Dessert et al. (2015) and Mg/Ca ratios used for throughfall (blue box), bulk soil (brown box) and Saharan dusts (yellow box) are from Clergue et al. (2015).

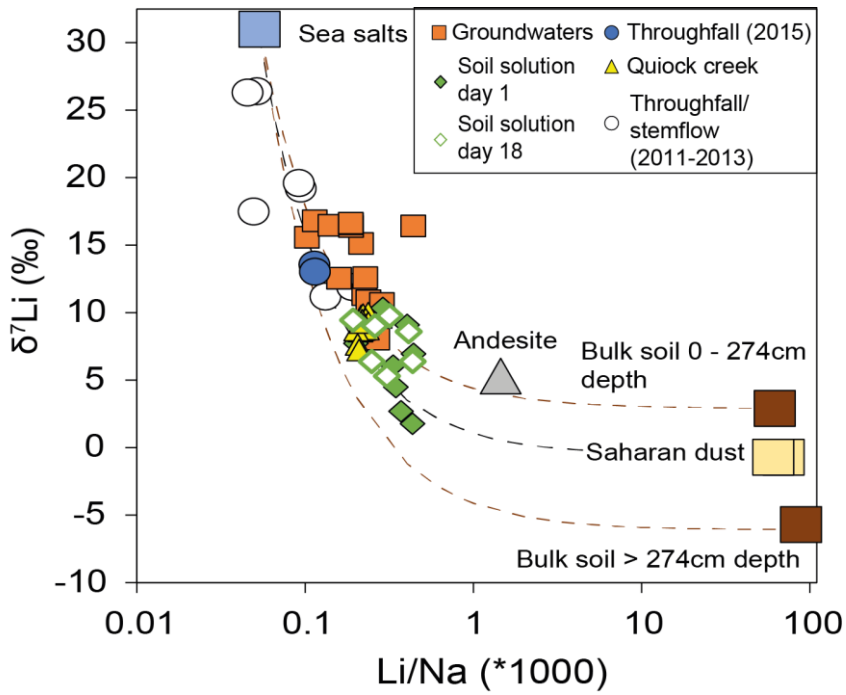

Figure 9. δ^7Li versus Li/Na for all fluids from Quiock Creek catchment. δ^7Li values for andesite, throughfall/stemflow (collected in 2011-2013), and bulk soils are from Clergue et al. (2015). Dashed lines represent the theoretical mixing trend between seawater and dust or bulk soils. The external error of the δ^7Li values is smaller than the symbols.

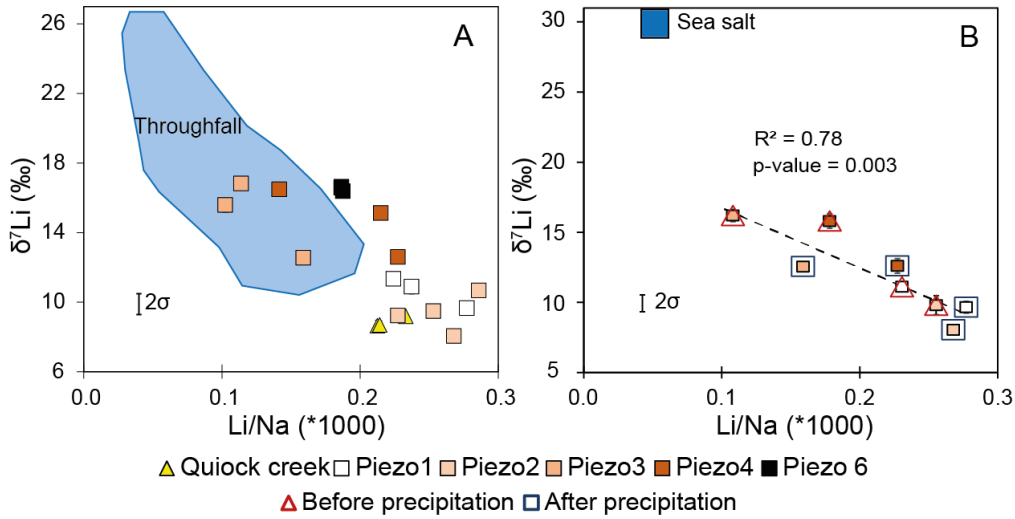

Figure 10. A. Relationship between δ^7Li vs Li/Na for the dissolved load in groundwaters and Quiock Creek samples sampled on Day 1, 4, 8, and 9 (Piezo 5 is not shown). The blue shaded area shows the throughfall/stemflow composition (Clergue et al., 2015). B. Li/Na versus δ^7Li in groundwaters before and after precipitation. The red open triangles show the average value for samples collected on Day 1 and 8 while the blue open squares show the values measured after a significant rain event at Day 9. The dashed line represents the linear evolution of Li/Na versus δ^7Li before and after precipitation.

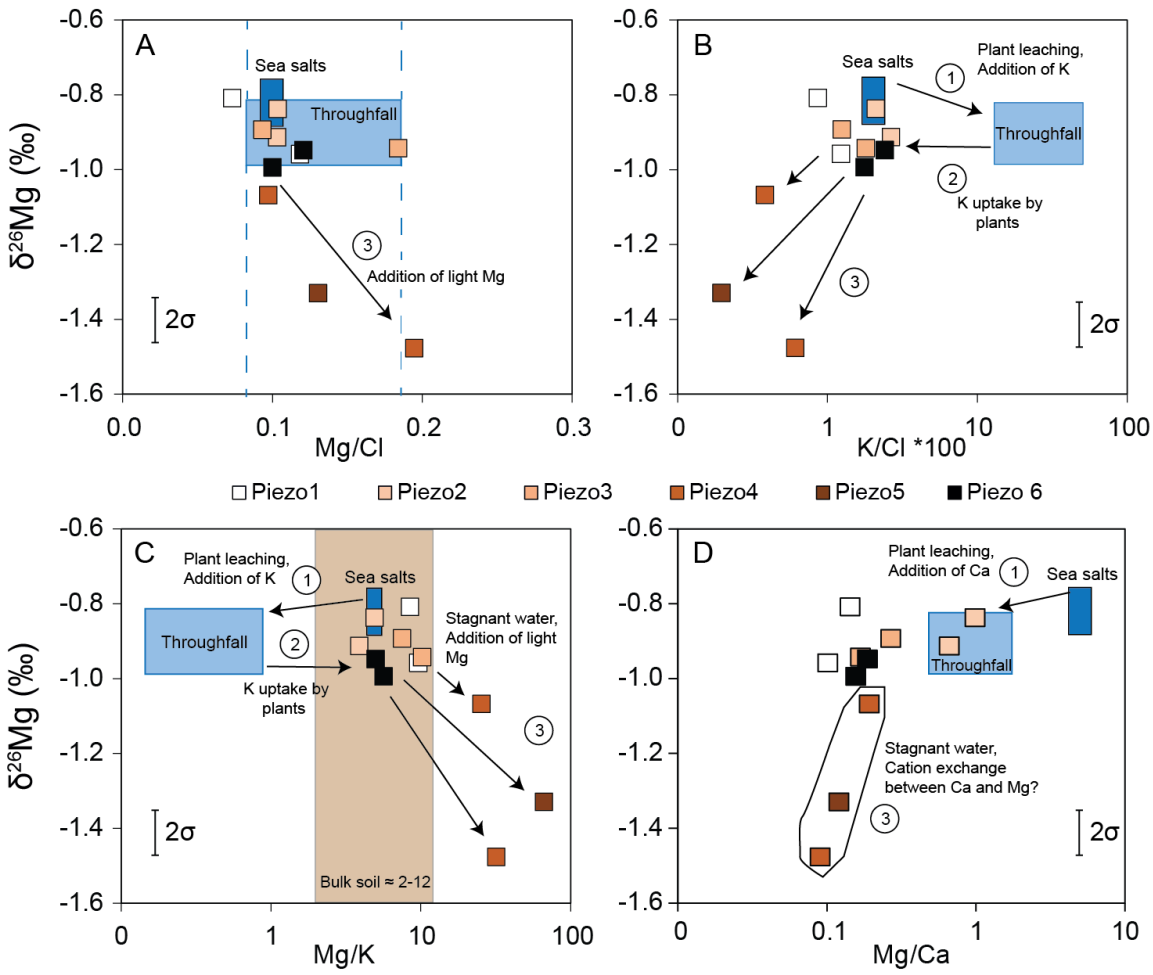

Figure 11. A. Relationship between δ^{26}Mg vs Mg/Cl, B. δ^{26}Mg vs K/Cl, C. δ^{26}Mg vs Mg/K and D. δ^{26}Mg vs Mg/Ca for the dissolved load in groundwaters. The light blue shaded box shows the throughfall composition while the dark blue shaded box shows the sea salt composition. The brown shaded box shows the composition range (Mg/K ratio) of bulk soil. Three different patterns are observed to explain change in K and Mg content together with δ^{26}Mg.

The response of Li and Mg isotopes to rain events in a highly-weathered catchment

David M. Fries[1], Rachael H. James[1], Céline Dessert[2], Julien Bouchez[2], Aurélien Beaumais[1, 3], Christopher R. Pearce[4]

[1]School of Ocean and Earth Science, National Oceanography Centre Southampton, University of Southampton Waterfront Campus, European Way, Southampton SO14 3ZH, UK

[2]Institut de Physique du Globe de Paris (IPGP), Sorbonne Paris Cité, Université Paris Diderot, CNRS, Paris, France

[3]DEN – Service d'Etudes Analytiques et de Réactivité des Surfaces (SEARS), CEA, Université Paris-Saclay, F-91191 Gif sur Yvette, France

[4]Marine Geoscience, National Oceanography Centre, Southampton SO14 3ZH, UK

Manuscript Tables 1-5

Table 1. Sample terminology.

Sample	Description	X	Y
L X.Y	Lysimeter/Soil solution	Depth (61 to 1250 cm)	Collection day (1 or 18)
Th X	Throughfall	Location	-
Piezo X.Y	Piezometer/Groundwater	Location (1 to 6)	Collection day (1, 4, 8 or 9)
QC Y	Quiock Creek/River water	-	Collection day (1 to 21)

Table 2. Field measurements and alkalinity data for Quiock Creek catchment samples. n.d = not determined, b.d = below detection limit. Discharge data are from the ObsERA website (http://webobsera.ipgp.fr/).

Sample	Day	Date	Distance to river (m)	Temperature (°C)	pH	Conductivity (µS/cm)	Alkalinity (µeq/L)
Soil solution							
L91.18	18	23/10/2015	-	n.d	4.9	n.d	b.d
L152.1	1	06/10/2015	-	n.d	5.2	n.d	18
L152.18	18	23/10/2015	-	n.d	5.2	n.d	5
L274.1	1	06/10/2015	-	n.d	4.9	n.d	b.d
L274.18	18	23/10/2015	-	n.d	4.7	n.d	b.d
L344.1	1	06/10/2015	-	n.d	4.8	n.d	b.d
L344.18	18	23/10/2015	-	n.d	4.5	n.d	b.d
L457.1	1	06/10/2015	-	n.d	5.5	n.d	22
L457.18	18	23/10/2015	-	n.d	5.2	n.d	9
L823.1	1	06/10/2015	-	n.d	5.1	n.d	8
L823.18	18	23/10/2015	-	n.d	4.8	n.d	b.d
Throughfall							
Th1	11	16/10/2015	-	25.4	5.9	42	67
Th3	11	16/10/2015	-	25.4	5.9	42	28
Groundwaters							
Piezo 1.1	1	06/10/2015	1.0	24.9	6.1	92	597
Piezo 1.4	4	09/10/2015	1.0	24.8	6.5	77	297
Piezo 1.8	8	13/10/2015	1.0	24.5	6.0	68	254
Piezo 2.1	1	06/10/2015	2.4	25.3	5.6	49	28
Piezo 2.4	4	09/10/2015	2.4	25.9	5.3	60	13
Piezo 2.8	8	13/10/2015	2.4	24.6	4.9	48	15
Piezo 2.9	9	14/10/2015	2.4	24.6	4.8	49	5
Piezo 3.1	1	06/10/2015	4.5	24.5	6.3	105	691
Piezo 3.8	8	13/10/2015	4.5	24.5	6.4	109	529
Piezo 3.9	9	14/10/2015	4.5	24.7	5.8	72	187
Piezo 4.1	1	06/10/2015	9.4	24.2	6.4	149	1108
Piezo 4.8	8	13/10/2015	9.4	24.1	6.0	94	566
Piezo 4.9	9	14/10/2015	9.4	24.4	5.6	65	238
Piezo 5.1	1	06/10/2015	21.2	24.4	6.3	94	579
Piezo 6.1	1	06/10/2015	29.8	24.2	5.7	65	315
Piezo 6.8	8	13/10/2015	29.8	n.d	n.d	n.d	n.d
Piezo 6.9	9	14/10/2015	29.8	24.7	5.6	53	214
Sample	**Day**	**Date**	**Discharge (m^3/h)**	**Temperature (°C)**	**pH**	**Conductivity (µS/cm)**	**Alkalinity (µeq/L)**
Quiock Creek							
QC1	1	06/10/2015	0.8	25.5	5.5	53	b.d
QC2	2	07/10/2015	0.8	25.3	5.5	48	1
QC3	3	08/10/2015	0.8	25.5	5.6	52	8
QC4	4	09/10/2015	0.8	25	5.5	52	7
QC5	5	10/10/2015	1.2	25	5.6	49	5
QC6	6	11/10/2015	1.5	24.7	5.3	55	b.d
QC7	7	12/10/2015	0.8	24.9	5.3	56	b.d
QC8	8	13/10/2015	0.5	24.4	5.3	52	10
QC9	9	14/10/2015	7.3	24.7	5.1	48	6
QC10	10	15/10/2015	1.7	24.8	5.2	50	3
QC11	11	16/10/2015	6.9	24.5	5.1	48	5
QC12	12	17/10/2015	14.3	24.2	5.1	45	1
QC13	13	18/10/2015	3.1	23.7	5.2	46	2
QC14	14	19/10/2015	1.8	23.8	5.2	46	b.d
QC15	15	20/10/2015	1.6	23.9	5.2	47	5
QC16	16	21/10/2015	1.2	24.7	5.3	48	7
QC17	17	22/10/2015	1.5	25	5.5	48	1
QC18	18	23/10/2015	1.4	24.1	5.1	48	b.d
QC19	19	24/10/2015	1.2	24.2	5.2	47	0.1
QC20	20	25/10/2015	88.8	24.3	4.9	35	b.d
QC21	21	26/10/2015	7.7	24.5	4.9	42	0.4

Table 3. Concentrations of major and minor elements in soil solution, groundwater, throughfall and Quiock Creek itself. n.d = not determined, b.d = below detection limit. TDS* = Total Dissolved Solids, calculated as the sum of cation, anion and Si concentrations in ppm.

Sample	µmol/kg										nmol/kg		TDS*
	Cl^-	SO_4^{2-}	Na^+	Ca^{2+}	Si	Mg^{2+}	K^+	Al	B	Fe	Sr	Li	
Soil solution													
L61.1	n.d	n.d	142	7.5	86	18.0	3.0	5.3	2.4	b.d	53	47	-
L61.18	n.d	n.d	207	11.3	67	25.6	4.5	6.7	3.6	b.d	76	54	-
L91.1	n.d	n.d	185	4.5	92	18.3	3.1	3.3	1.5	b.d	19	69	-
L91.18	264	9.3	230	6.1	68	24.2	4.1	3.9	2.1	b.d	21	57	19
L152.1	206	11.7	145	5.4	45	19.4	2.1	3.2	0.8	b.d	14	29	15
L152.18	207	12.3	179	3.7	52	24.4	1.9	4.6	1.0	b.d	13	34	15
L274.1	244	12.5	168	1.2	65	20.4	2.9	9.3	2.4	b.d	15	68	16
L274.18	253	14.4	204	2.4	78	24.5	3.6	9.4	2.8	b.d	21	84	18
L344.1	388	15.0	247	1.0	75	42.8	7.1	12.7	2.3	b.d	16	71	25
L344.18	360	17.1	255	1.6	87	42.6	7.8	11.4	2.4	b.d	18	81	24
L457.1	184	11.4	178	1.2	102	9.9	3.5	5.5	0.8	b.d	10	79	16
L457.18	195	14.8	202	1.8	106	11.5	3.8	5.3	1.0	b.d	13	88	17
L823.1	264	16.6	231	1.5	113	14.0	14.2	6.5	0.9	b.d	14	80	21
L823.18	271	18.5	253	1.6	106	15.4	15.3	6.6	1.0	b.d	14	77	21
L1250	n.d	n.d	220	2.8	153	24.8	34.9	1.8	0.9	b.d	12	95	-
Throughfall													
Th1	n.d	7.1	123	20.9	18	18.4	66.7	2.9	3.0	0.6	64	14	-
Th3	144	15.4	121	18.2	26	13.6	30.6	2.5	3.0	0.5	55	14	14
Groundwater													
Piezo 1.1	259	25.9	222	302	58	30.6	3.2	2.5	1.5	3.7	232	50	62
Piezo 1.4	278	23.0	197	178	60	22.3	2.4	0.6	1.4	1.7	160	47	41
Piezo 1.8	285	16.4	198	145	68	20.8	2.5	0.9	1.4	0.2	151	55	37
Piezo 2.1	255	29.8	209	40	69	26.2	6.8	10.8	2.1	5.9	88	47	23
Piezo 2.4	260	27.3	198	32	68	25.8	5.9	3.9	1.9	3.2	119	56	21
Piezo 2.8	261	27.1	196	30	69	25.7	5.6	3.5	1.9	6.5	95	50	22
Piezo 2.9	259	26.3	201	27	64	26.8	5.5	9.7	2.0	5.3	100	54	21
Piezo 3.1	295	35.1	305	322	41	54.2	5.3	7.5	1.3	4.5	187	31	71
Piezo 3.8	328	25.6	254	284	41	40.3	3.9	3.0	1.3	2.4	179	29	60
Piezo 3.9	335	18.6	233	116	44	31.2	4.2	8.3	1.5	0.6	121	37	35
Piezo 4.1	248	31.5	252	534	40	48.2	1.5	1.1	2.3	0.2	99	36	97
Piezo 4.8	269	20.0	208	270	48	31.1	1.5	2.2	1.8	1.1	77	45	58
Piezo 4.9	261	22.0	194	132	48	25.4	1.0	2.1	1.4	4.2	51	44	35
Piezo 5.1	259	25.4	209	279	43	33.7	0.5	4.2	1.3	3.5	127	92	59
Piezo 6.1	231	25.3	197	148	43	23.0	4.1	1.8	1.7	2.2	90	37	39
Piezo 6.8	n.d	n.d	190	193	47	26.7	3.8	n.d	1.9	n.d	133	35	-
Piezo 6.9	174	29.3	170	112	48	20.9	4.2	11.9	2.4	2.8	85	32	31
Quiock Creek													
QC1	334	10.0	257	12.8	89	27.0	9.0	2.1	1.6	0.3	57	55	23
QC2	333	9.8	258	13.1	90	27.5	6.2	2.0	1.6	0.2	67	55	23
QC3	336	9.6	260	13.1	91	27.8	6.5	2.1	1.5	0.3	64	56	23
QC4	350	11.0	261	14.0	88	28.4	6.7	2.5	1.7	0.3	79	56	24
QC5	326	13.5	247	13.3	83	27.5	9.3	3.4	1.8	0.4	68	56	23
QC6	332	12.5	241	12.7	80	26.7	8.3	3.4	1.8	0.4	64	52	22
QC7	335	11.0	246	13.0	86	27.1	7.5	4.0	1.7	0.4	65	53	23
QC8	327	10.5	240	13.0	83	26.6	7.5	3.0	1.7	0.4	64	53	23
QC9	328	11.3	255	11.5	82	26.4	7.0	3.3	1.7	0.4	60	59	23
QC10	317	13.8	255	13.6	81	27.8	8.1	4.9	1.9	0.7	78	60	23
QC11	319	10.7	250	11.8	79	26.7	6.1	3.8	1.7	0.6	60	57	22
QC12	307	11.8	249	12.1	69	27.9	4.9	3.8	1.8	0.6	66	58	21
QC13	321	9.3	251	12.1	77	27.6	4.8	1.8	1.6	0.2	62	55	22
QC14	325	9.9	261	13.1	87	28.9	5.4	1.8	1.6	0.2	75	62	22
QC15	326	9.9	257	12.4	90	28.4	5.2	2.6	1.5	0.2	63	56	23
QC16	326	10.1	262	12.8	92	28.4	5.4	1.8	1.5	0.2	66	58	23
QC17	328	10.1	263	13.3	91	28.3	6.3	2.3	1.6	0.2	78	61	23
QC18	330	11.0	271	12.6	92	28.8	6.5	2.6	1.6	0.4	58	54	23
QC19	330	10.4	269	12.8	98	29.3	5.8	2.2	1.5	0.3	65	58	23
QC20	226	18.3	201	10.9	61	22.0	4.8	8.0	2.0	1.5	56	41	18
QC21	297	13.2	245	11.3	73	26.6	4.3	2.1	1.7	0.3	61	51	21

Table 4. Li and Mg isotope compositions in soil solution, groundwater, throughfall and Quiock Creek itself. n.d = not determined. 2σ is the internal uncertainty of the sample measurements.

Sample	δ^{7}Li (‰)	2σ	δ^{25}Mg (‰)	2σ	δ^{26}Mg (‰)	2σ
Soil solution						
L61.1	6.1	0.5	-0.53	0.01	-0.95	0.00
L61.18	9.0	0.5	-0.54	0.03	-1.04	0.05
L91.1	2.7	0.2	-0.50	0.03	-0.94	0.05
L91.18	6.4	0.3	-0.48	0.01	-0.91	0.03
L152.1	7.7	0.5	-0.42	0.02	-0.78	0.04
L152.18	9.5	0.1	-0.48	0.04	-0.88	0.00
L274.1	9.1	0.1	-0.46	0.05	-0.82	0.04
L274.18	8.6	0.1	-0.41	0.03	-0.79	0.05
L344.1	10.4	0.5	-0.41	0.07	-0.77	0.06
L344.18	9.8	0.3	-0.37	0.01	-0.72	0.02
L457.1	7.0	0.1	-0.32	0.01	-0.63	0.01
L457.18	6.4	0.6	-0.36	0.03	-0.70	0.06
L823.1	4.5	0.1	-0.30	0.00	-0.58	0.02
L823.18	5.3	0.2	-0.32	0.03	-0.63	0.07
L1250	1.8	0.0	-0.33	0.01	-0.65	0.03
Throughfall						
Th1	13.6	0.2	-0.50	0.01	-0.97	0.02
Th3	13.0	0.0	-0.45	0.00	-0.84	0.04
Groundwater						
Piezo 1.1	11.3	0.1	-0.52	0.04	-0.96	0.06
Piezo 1.4	10.9	0.4	n.d	n.d	n.d	n.d
Piezo 1.8	9.7	0.2	-0.43	0.08	-0.81	0.04
Piezo 2.1	9.2	0.7	-0.48	0.02	-0.91	0.04
Piezo 2.4	10.7	0.1	n.d	n.d	n.d	n.d
Piezo 2.8	9.5	0.2	n.d	n.d	n.d	n.d
Piezo 2.9	8.0	0.1	-0.43	0.05	-0.84	0.06
Piezo 3.1	15.6	0.4	-0.49	0.01	-0.94	0.02
Piezo 3.8	16.8	0.0	n.d	n.d	n.d	n.d
Piezo 3.9	12.6	1.3	-0.45	0.00	-0.89	0.07
Piezo 4.1	16.5	0.5	-0.78	0.02	-1.48	0.01
Piezo 4.8	15.1	0.3	n.d	n.d	n.d	n.d
Piezo 4.9	12.6	0.3	-0.56	0.02	-1.07	0.01
Piezo 5.1	16.4	0.2	-0.73	0.09	-1.33	0.10
Piezo 6.1	16.4	0.3	-0.51	0.03	-0.99	0.05
Piezo 6.8	16.6	0.2	n.d	n.d	n.d	n.d
Piezo 6.9	16.6	0.3	-0.48	0.05	-0.95	0.04
Quiock Creek						
QC1	8.6	0.3	-0.38	0.01	-0.72	0.02
QC2	9.8	0.4	-0.38	0.02	-0.73	0.05
QC3	9.2	0.1	-0.38	0.01	-0.73	0.01
QC4	8.7	0.2	n.d	n.d	n.d	n.d
QC5	9.1	0.6	n.d	n.d	n.d	n.d
QC6	9.8	0.1	-0.44	0.03	-0.85	0.06
QC7	9.7	0.4	n.d	n.d	n.d	n.d
QC8	9.9	0.1	-0.41	0.01	-0.77	0.02
QC9	9.2	0.1	-0.41	0.06	-0.80	0.05
QC10	10.0	0.2	-0.38	0.00	-0.74	0.03
QC11	9.5	0.1	n.d	n.d	n.d	n.d
QC12	9.1	0.1	-0.45	0.01	-0.87	0.01
QC13	8.8	0.3	-0.43	0.01	-0.84	0.01
QC14	9.2	0.3	n.d	n.d	n.d	n.d
QC15	9.5	0.1	n.d	n.d	n.d	n.d
QC16	9.0	0.2	-0.43	0.03	-0.84	0.03
QC17	8.8	0.0	n.d	n.d	n.d	n.d
QC18	8.7	0.1	n.d	n.d	n.d	n.d
QC19	9.3	0.0	n.d	n.d	n.d	n.d
QC20	7.7	0.2	-0.40	0.01	-0.76	0.03
QC21	7.2	0.6	-0.40	0.06	-0.77	0.06

Table 5. Elemental contribution (%) of sea salts in Quiock Creek catchment fluids where $(Mg/Cl)_{sea}$ = 0.1, $(Ca/Cl)_{sea}$ = 0.02, $(K/Cl)_{sea}$ = 0.02 and $(Na/Cl)_{sea}$ = 0.86 (Dessert et al., 2015).

X	Amount derived from sea salt (%)									
	Li		Mg		Ca		K		Na	
	Min	Max	Min	Max	Min	Max	Min	Max	Min	Max
Soil solution	10	33	85	100	76	100	35	100	83	100
Throughfall	44	48	77	100	13	16	4	9	94	100
Groundwaters	13	52	51	100	1	19	75	100	83	100
Quiock Creek	24	29	100	100	41	57	70	100	96	100

The response of Li and Mg isotopes to rain events in a highly-weathered catchment

David M. Fries[1], Rachael H. James[1], Céline Dessert[2], Julien Bouchez[2], Aurélien Beaumais[1, 3], Christopher R. Pearce[4]

[1]School of Ocean and Earth Science, National Oceanography Centre Southampton, University of Southampton Waterfront Campus, European Way, Southampton SO14 3ZH, UK

[2]Institut de Physique du Globe de Paris (IPGP), Sorbonne Paris Cité, Université Paris Diderot, CNRS, Paris, France

[3]DEN – Service d'Etudes Analytiques et de Réactivité des Surfaces (SEARS), CEA, Université Paris-Saclay, F-91191 Gif sur Yvette, France

[4]Marine Geoscience, National Oceanography Centre, Southampton SO14 3ZH, UK

Appendix/ Supplementary Figures A1-A7

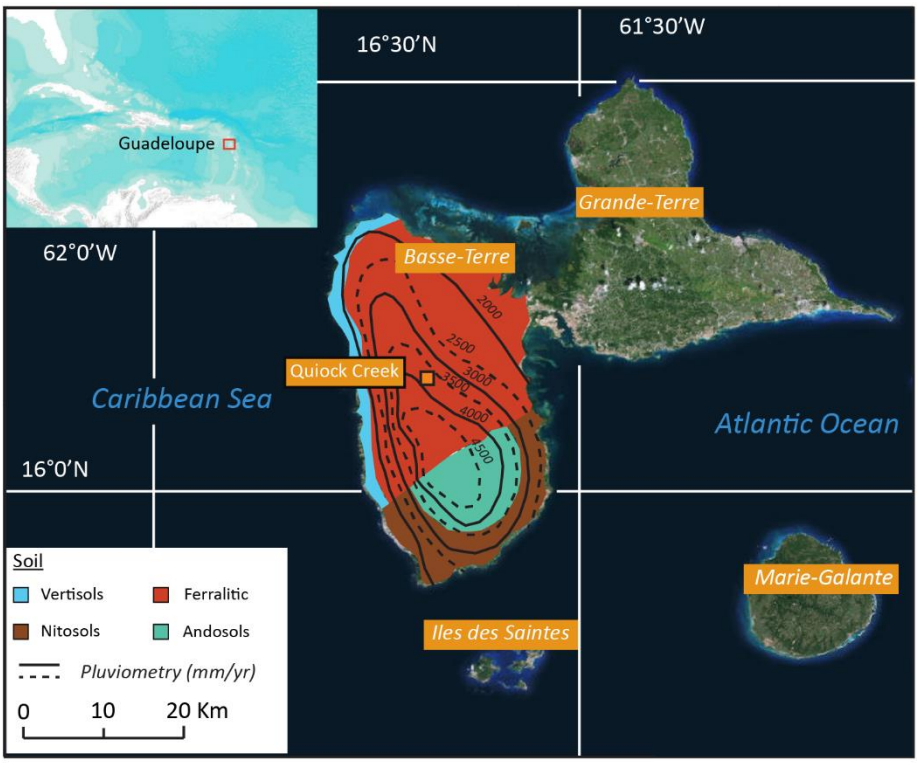

Figure A 1. Location of Quiock Creek catchment (orange square; 16°17'N, 61°60'W) in Guadeloupe with isohyets (adapted from Lloret et al., 2010) and simplified map of Guadeloupe soils (adapted from Colmeet-Daage and Bernard, 1979).

The hydrological conditions of Quiock Creek catchment since the soil solution reservoirs were first emptied is reported here. A description of these conditions is necessary to accurately interpret the soil solution and groundwater chemistry of the sample collected during the first day of the campaign. Briefly, during this period a relatively small input of rainfall entered the catchment (~36.4 mm over 18 days) and therefore the water table elevation decreased and discharge was relatively low (maximum of 12m^3/h on 28/09/15). The water table in Piezo 1, 2 and 3 was below the river elevation at the beginning of the study.

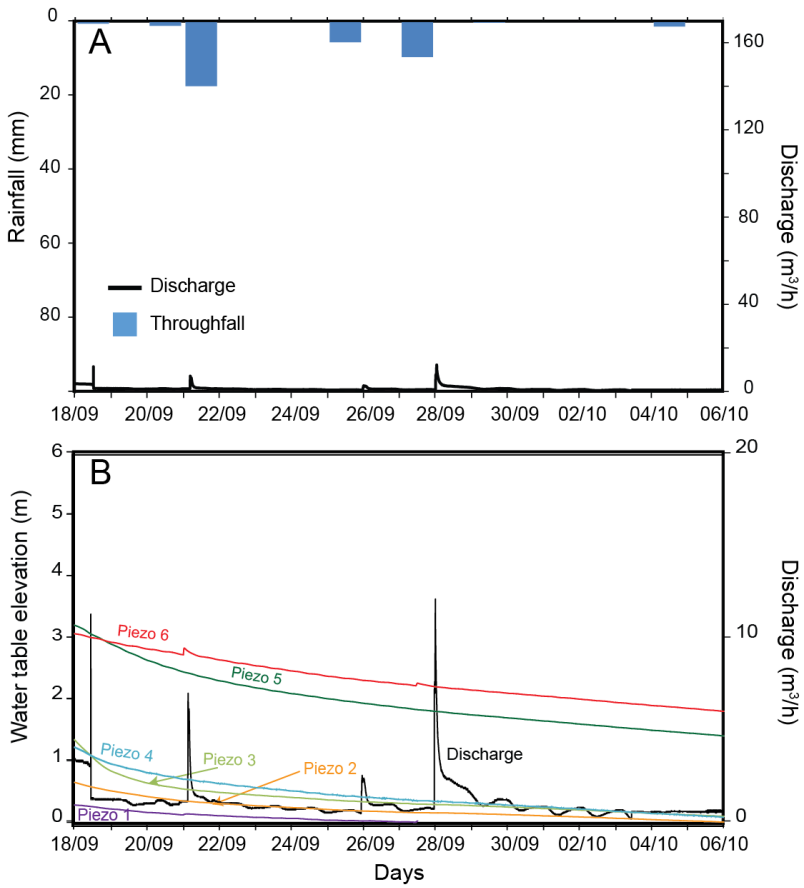

Figure A 2. A. Precipitation and discharge of Quiock Creek. B. Water table elevation and discharge from the 18/09/2015 until the beginning of the sampling campaign. All the discharge and water elevation data are from the ObsERA website (http://webobsera.ipgp.fr/).

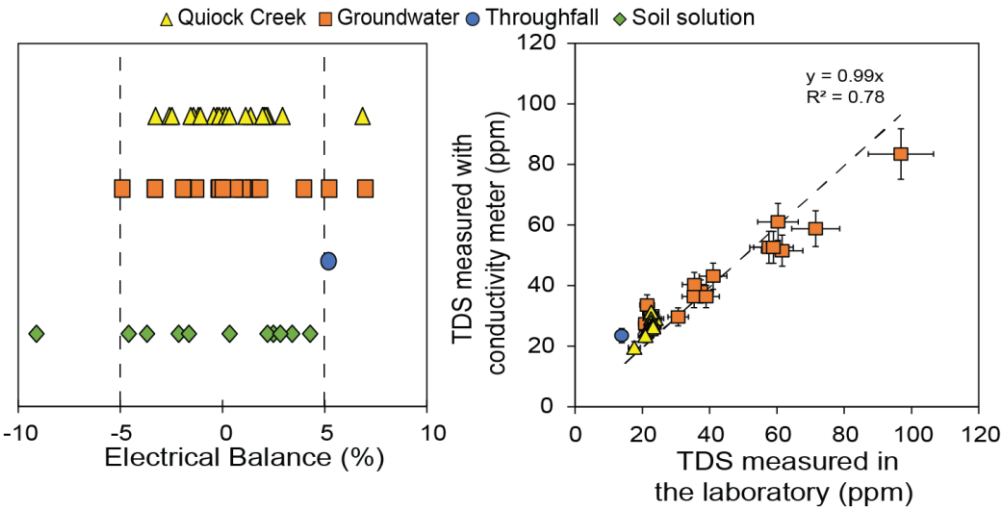

Figure A 3. (a) Electrical balance and (b) TDS measured using a conductivity meter vs TDS measured in the laboratory for Quiock Creek samples.

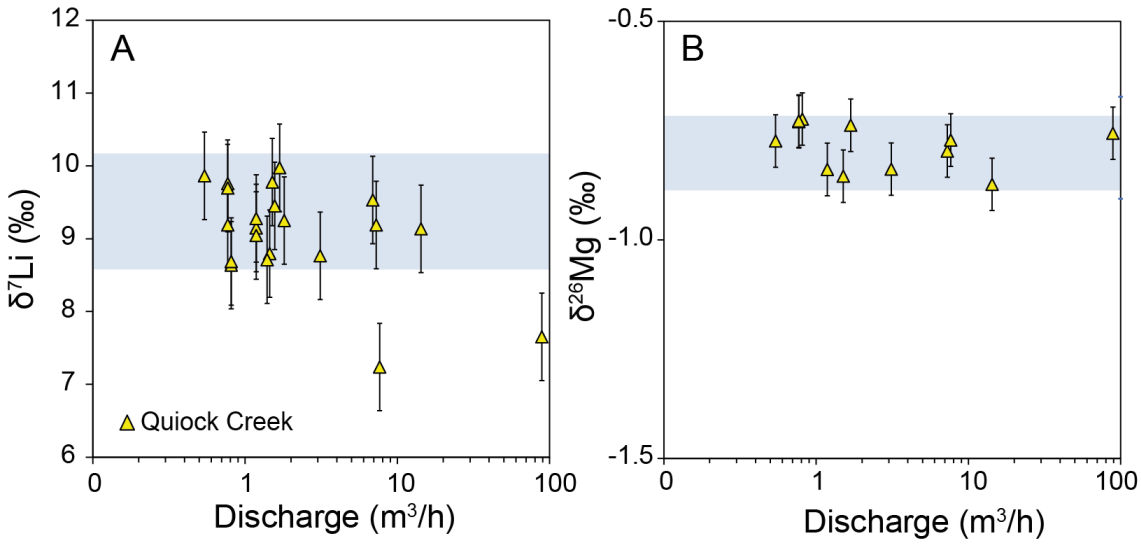

Figure A 4. A. δ^{7}Li vs discharge. B. δ^{26}Mg vs discharge. Blue shaded boxes show the range of δ^{7}Li and δ^{26}Mg measured before the storm (QC20 and QC21 excluded from the average). Error bars show the external error of the isotope measurements.

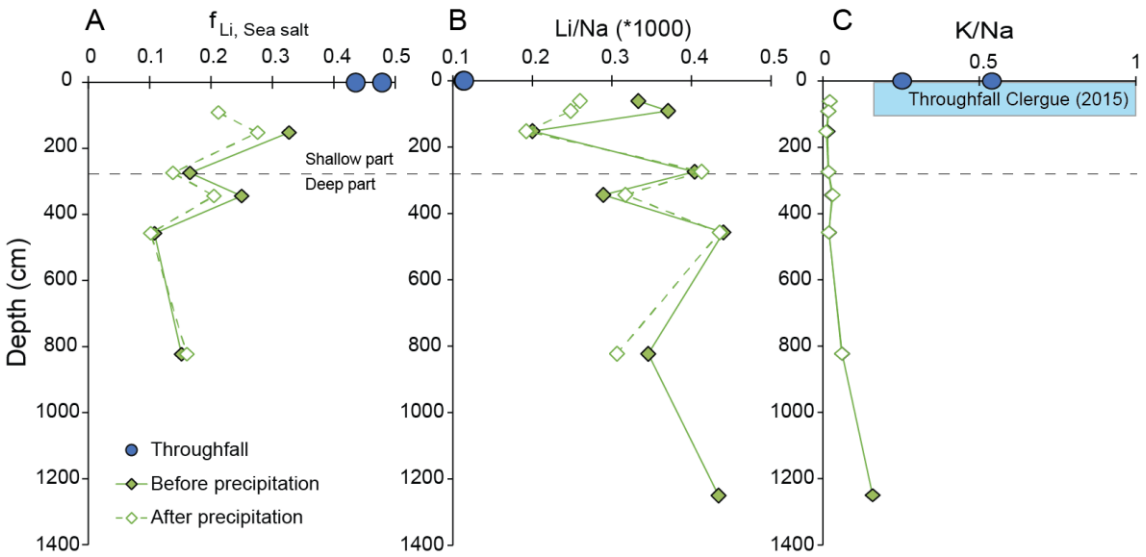

Figure A 5. A. Fraction of Li derived from sea salts in the soil solutions. B and C. Evolution of soil solution Li/Na and K/Na with depth before and after rainfall events. C. The blue shaded box shows the range of K/Na in throughfall samples measured by Clergue et al. (2015).

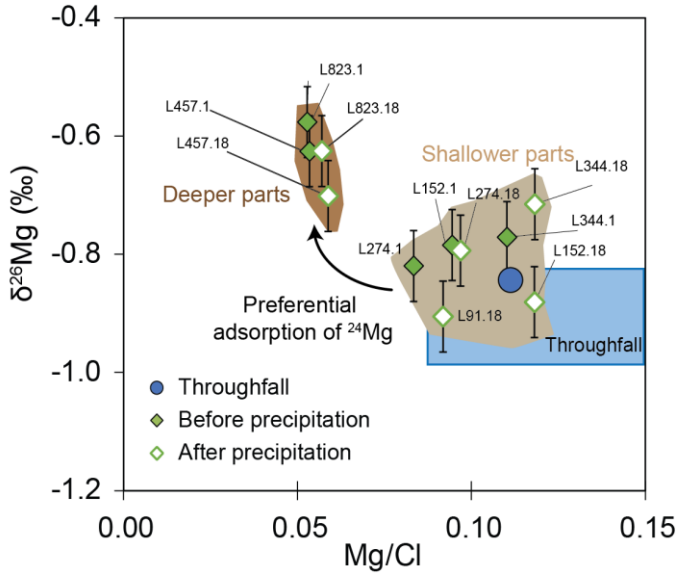

Figure A 6. Mg/Cl versus δ^{26}Mg in the soil solution before and after rainfall events. The figure highlights the removal of Mg from the solution in the deeper part of the profile together with an increase of δ^{26}Mg. The blue shaded box shows the throughfall/stemflow composition (Clergue et al., 2015).

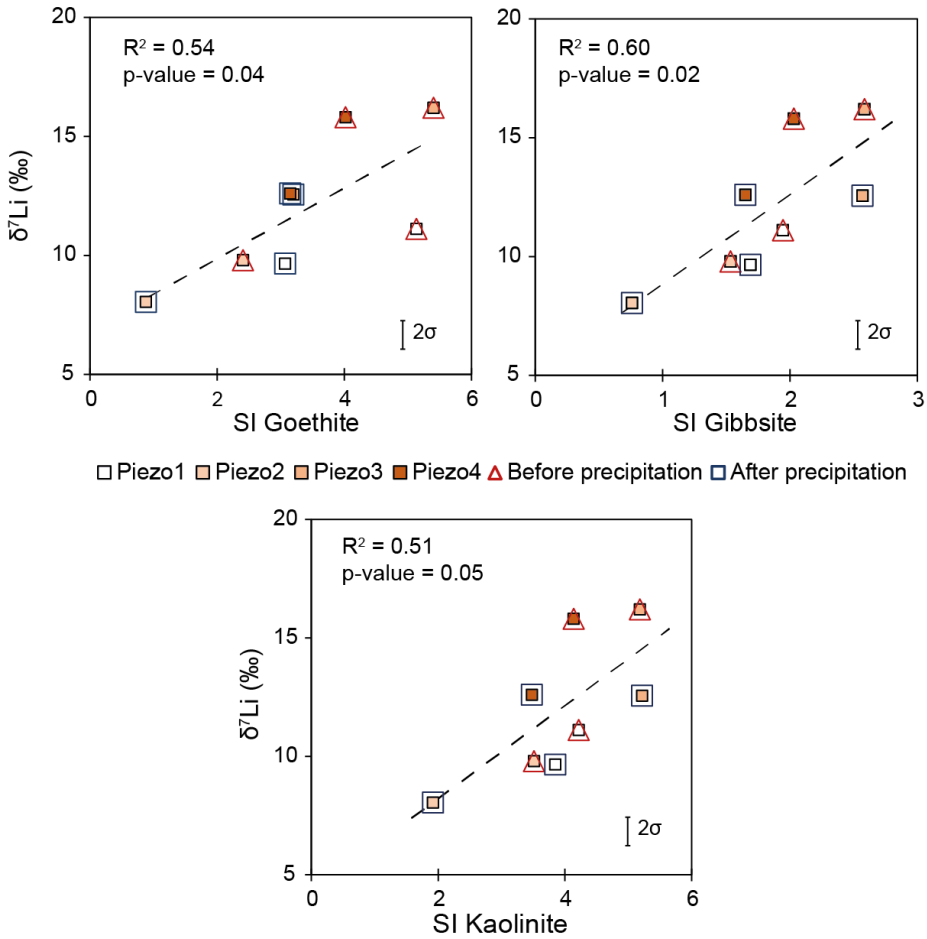

Figure A 7. δ^7Li vs saturation index (SI) of goethite, gibbsite and kaolinite in groundwaters. The red open triangles show the average value for samples collected on Day 1, 4 and 8 while the blue open squares show the value measured after a significant rain event at Day 9.